NORTH AMERICAN AVIATION, INC. SPACE and INFORMATION SYSTEMS DIVISION

Accession No. 00481-65

Copy No. 3

SID 65-44

ENGINEERING METHOD TO PREDICT SATURN V VEHICLE AND LAUNCH COMPLEX ENVIRONMENTS DUE TO ROCKET JET IMPINGEMENT

QUARTERLY PROGRESS REPORT NO. 2
Contract NAS 8-11407

15 JANUARY 1965

Prepared by
A. Africano
A. Africano

Power and Environmental Systems

Approved by

F. G. Etheridge
Program Manager

W. H. T. Loh, Director
Power and Environmental Systems
Aerospace Sciences Division

[redacted]

FOREWORD

This is the second quarterly progress report submitted to NASA/MSFC in partial fulfillment of the requirements of Contract NAS 8-11407. The report covers activity and progress achieved in the three-month report period 1 October through 31 December 1964. S&ID personnel contributing material used in the report include E. P. French (radiation), J. W. Rolley (convective heat transfer), R. J. Hoffman (jet plume free flow fields with varying specific heat ratio), and A. Africano (sea level plumes, plume impingement geometry, and general supervision). The scope covered includes principally the Phase II Analytical and Experimental correlation, with some remaining items from the Phase I Analytical Investigations. The next quarterly progress report is expected to complete the Phase II Correlation and begin the Phase III generation of the recommended Engineering Prediction Method. This study program is under the direction of J. C. Cody, NASA/MSFC Contracting Officer's Representative, and J. L. Moses, Alternate, of the George C. Marshall Space Flight Center, Propulsion and Vehicle Engineering Division, Huntsville, Alabama. F. G. Etheridge is the Program Manager for NAA/S&ID.

TECHNICAL REPORT INDEX/ABSTRACT

ACCESSION NUMBER						DOCUMENT SECURITY CLASSIFICATION	
00481-65						Unclassified	

TITLE OF DOCUMENT

Engineering Method to Predict Saturn V Vehicle and Launch Complex Environments due to Rocket Jet Impingement, Quarterly Progress Report No. 2, Contract NAS 8-11407.

LIBRARY USE ONLY

AUTHOR(S)

A. Africano

CODE	ORIGINATING AGENCY AND OTHER SOURCES	DOCUMENT NUMBER
	NAA/S&ID Aerospace Sciences	SID 65-44

PUBLICATION DATE	CONTRACT NUMBER
15 January 1965	NAS 8-11407

DESCRIPTIVE TERMS

Rocket Jet Plume Environments
(Plume) Impact Pressure
(Plume) Radiation Heat Transfer
(Plume) Convective Heat Transfer
Saturn V Vehicle
Prediction Methods

ABSTRACT

This report presents the results obtained during the second three-month period of contract performance under NASA/MSFC Contract NAS 8-11407. The twelve-month study comprises three phases, each of approximately four months duration. The material in this report falls principally within the Phase II Analytical and Experimental Correlation portion of the overall study. The objective of the study is to correlate available experimental data with theoretical and empirical relations to arrive at a comprehensive engineering method for predicting force and heat load environments due to rocket jet impingement on space vehicles or nearby structures represented by flat and curved surfaces.

Topics discussed include:

1. A summary of the principal topics covered in Quarterly Progress Report No. 1.
2. Jet plume free flow fields as affected by choice of a fixed or shifting exhaust gas specific heat ratio.
3. Interaction of the moving jet plume with air at different freestream Mach numbers.
4. Approximation of a sea level jet plume and its application in correlating the impingement and thermal load test data from SA5 and SA6 launches.
5. Convective heat transfer correlation for high altitude plumes.
6. Solid particle effects in plume radiation.

SUMMARY

This report presents the results obtained during the second three-month period of contract performance under NASA/MSFC Contract NAS 8-11407. The twelve-month study comprises three phases, each of approximately four months duration. The material in this report falls principally within the Phase II Analytical and Experimental Correlation portion of the overall study. The objective of the study is to correlate available experimental data with theoretical and empirical relations to arrive at a comprehensive engineering method for predicting force and heat load environments due to rocket jet impingement on space vehicles or nearby structures represented by flat and curved surfaces.

Topics discussed include:

(1) A summary of the principal topics covered in Quarterly Progress Report No. 1.

(2) Jet plume free flow fields as affected by choice of fixed or shifting exhaust gas specific heat ratio.

(3) Interaction of the moving jet plume with air at different free-stream Mach numbers.

(4) Approximation of a sea level jet plume and its application in correlating the impingement and thermal load test data from SA5 and SA6 launches.

(5) Convective heat transfer correlation for high altitude plumes.

(6) Solid particle effects in plume radiation.

TABLE OF CONTENTS

ILLUSTRATIONS

TABLES

I. INTRODUCTION

This is the second quarterly progress report submitted by North American Aviation, Inc., Space and Information Systems Division (NAA/S&ID) to the National Aeronautics and Space Administration, George C. Marshall Space Flight Center (NASA/MSFC) on Contract NAS 8-11407 covering the contract performance period 1 October 1964 through 31 December 1964. The program is a twelve-month investigation of the correlation between theoretical or empirical prediction procedures and the available experimental data on rocket jet plume impingement forces and heat loads. The structures affected by the plume impingement may be on the vehicle itself, other nearby vehicles, or the launch tower; however, all cases are categorized and simplified by considering impingement effects only on flat or curved surfaces at various distances aft or radially displaced from the centerline of the jet plume.

The Saturn V Vehicle and Launch Complex is utilized as a reference configuration (as illustrated in the first quarterly progress report, Reference (1)). The "Statement of Work" is also given in detail in the first quarterly report, together with a discussion of the environments before and after launch, and a general description of the Saturn V solid and storable propellant rocket engines involved and their locations in the vehicle.

The theoretical prediction methods accumulated to date have yielded results giving good correlation for both impact pressures and heat transfer rates due to plume impingement when compared with available high altitude chamber test data. High-altitude plumes are simpler to calculate and result in simpler impingement environments than low altitude plumes, and better correlation. The successful application of the methods depends, of course, on the accurate representation of the jet plume flow field and properties at the altitude under consideration. In view of the need for investigation of the effects during launch, it was agreed to apply the presently available prediction methods in an analysis of two of the data points for this case as requested in the NASA/MSFC letter dated 2 December 1964 (Reference 2). The principal problem in such an analysis is to estimate the properties of an (on the average) overexpanded rocket jet plume for the cryogenic booster engines at the sea level environment. Available dimensionless pressure, velocity, and temperature decay ratios from the NADC work of Anderson and Johns canbe used as a first approximation to determine this plume. The method is briefly described and the necessary decay ratios tabulated and utilized in the present report for a preliminary analysis.

A summary of the topics covered in the first quarterly progress report (Reference 1) follows as an aid in maintaining continuity.

I. Introduction - Program Objectives (reviewed above)

II. Basic Surface Environments of Space Vehicles and Launch Complex Structures (reviewed above)

III. Jet Plume Free Flow Fields (The Latvala circular arc approximation and more "exact" methods of characteristics solutions in use at NAA/S&ID are described and an example of the plume properties presented in a tabulated condensed version.)

IV. Interaction of Free Stream with Jet Plume (The basic relations needed to account for the contraction of the free flow field plume resulting from Newtonian impact on the inviscid gas boundary are described.)

V. Plume Impingement Geometry for Canted and Uncanted Side Plates (The equations for determination of the true impingement angle of a streamline on an element of area at any distance and orientation from the reference nozzle exit center are derived.)

VI. Newtonian Impact Theory for Impingement on a Flat Plate (The fundamental principle is emphasized that rate of change of momentum per unit area is the basis for predicting impingement pressures, and an equation is derived relating such pressures to the plume Mach number, specific heat ratio, total pressure, pressure expansion ratio, and the true streamline impingement angle.)

VII. Convective Heat Transfer Due to Jet Impingement (The available laminar flow heat transfer equations from prior aerodynamic heating theory are described.)

VIII. Plume Radiation Study (A method of computing total radiant power incident on a surface element from an axisymmetric exhaust plume is described.)

II. JET PLUME FREE FLOW FIELD WITH VARYING SPECIFIC HEAT RATIO

Due to the complexity of the method of characteristics solution, it has been the usual practice to assume some "effective" gas specific heat ratio at the nozzle exit plane, or nozzle lip (e.g., 1.25 to 1.30) and keep this constant for the plume calculation. This provided a marked improvement in the shape and location of the plume boundary over the earlier poor assumption of the very low combustion chamber equilibrium value remaining constant throughout the expansion in the nozzle and in the plume. However, since the specific heat ratio of all rocket propellant exhaust gases continues to increase as the expanding gas temperature decreases, even though the gas composition may effectively become stably "frozen" shortly downstream of the nozzle throat, some uncertainty remained as to the error involved by the use of the constant nozzle exit or lip value.

A full right running characteristic from the nozzle lip to the nozzle axis with the corresponding varying specific heat ratio values is required as input for the determination of the improved plume with this variable considered.

This right-running characteristic can be obtained from Rocketdyne's Kernel and Bell Analysis Program (on file at NAA/S&ID as 7N-202) for this purpose for conical nozzles. For the Saturn S-II J-2 engines, unfortunately, only a partial starting line was obtained by this program because it does not handle the internal shocks occurring in sharply contoured nozzles. This right running characteristic for the J-2 engine was computed for the following assumed conditions:

(a) ratio of specific heats constant at 1.23,
(b) nozzle area ratio, 27.45,
(c) J-2 contour,
(d) chamber pressure, 632 psia
(e) ratio of radius of curvature at throat to throat radius, 0.392.

The three J-2 cases calculated to determine the effect of the varying specific heat ratio on the plume include:

(a) chemical equilibrium
(b) frozen chamber composition
(c) an approximation to the exact finite-rate solution based on equilibrium flow up to a "freezing point," and then "freezing point" composition thereafter.

The first two cases utilized equilibrium composition properties and frozen chamber composition properties computed by a program obtained from NASA-Lewis and on file at NAA/S&ID as No. 7N-219. The "freezing point" analysis was obtained from a Rocketdyne program similar to the NASA-Lewis

program, but with the added refinement of allowing the composition to shift until predetermined "freezing point" criteria are satisfied, and then freezing the composition as the expansion continues. Some extrapolation below the temperature of 200°K was necessary in all cases. The common altitude assumed for the plumes was 200,000 ft. Also, a still atmosphere and inviscid flow were assumed.

Figures 1 to 3 show the resulting J-2 plumes for the three assumed conditions of shifting specific heat ratio. For comparison, Figure 4 is included based on a constant value of 1.28. Figure 5 is a composite of the four plume boundaries, showing an apparently appreciable displacement of the constant specific ratio plume from the other three which practically coincide. Impingement effects from such tenuous gas exhaust at 200,000 ft, however, may be negligible even with widely displaced boundaries. Therefore, an additional composite is included in Figure 5 of the Mach 9 and 6 streamlines. These are close enough together to indicate that the impingement errors due to assumption of a constant specific heat ratio might be negligibly small. Figure 6 is included to clarify the earlier discussion on the effect of an incomplete starting right running characteristic line.

The constant value of 1.28 is representative of the average specific heat ratio for the J-2 engine nozzle with its 27.5 area expansion ratio. Lower values of the order of 1.23 to 1.25 would be typical for lower expansion ratios, while 1.32 has been used for computing plumes for the very high expansion ratio of 40 in the Apollo SM/RCS engine.

Considering the greater effect of the free stream Mach No. on the free flow field jet plume (discussed in the next section of this report) it appears that the slight increase in accuracy by use of the shifting specific heat ratio may not be presently justified, although for high altitudes and for long plume firing durations, some special cases may benefit from or even require its use.

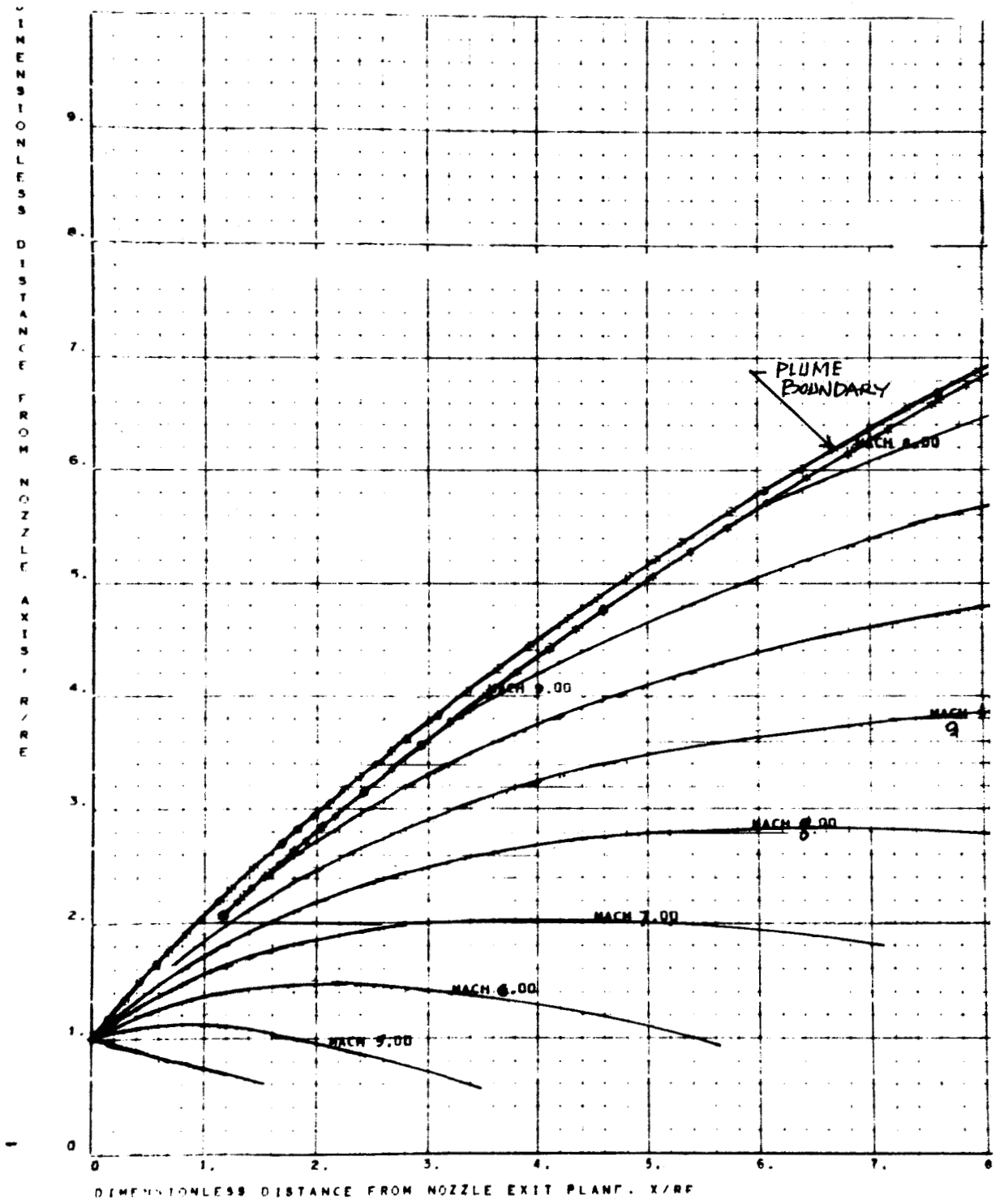

Figure 1: J-2 Plume at 200,000 ft, Equilibrium Composition

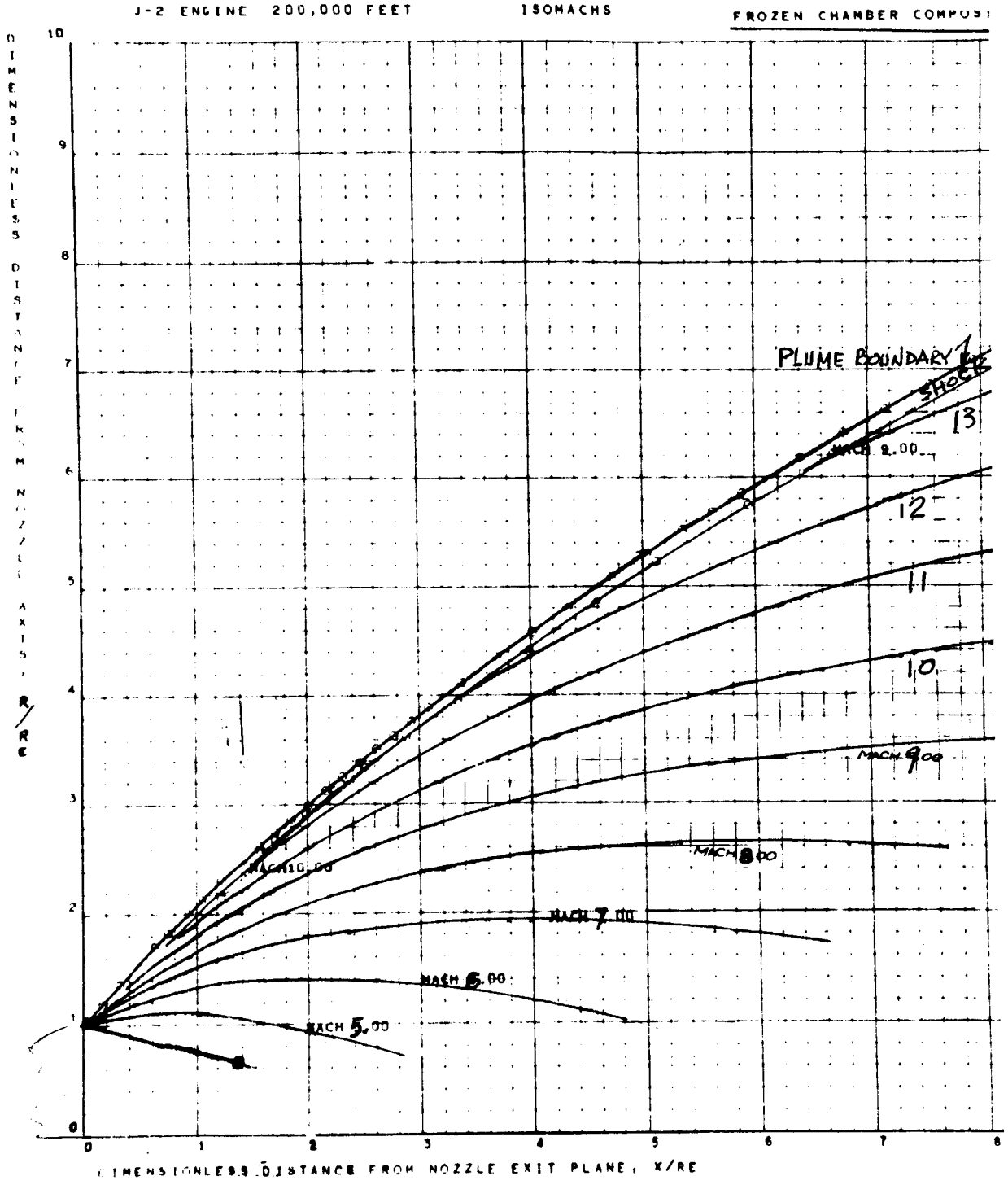

Figure 2: J-2 Engine Plume at 200,000 ft, Frozen Chamber Composition

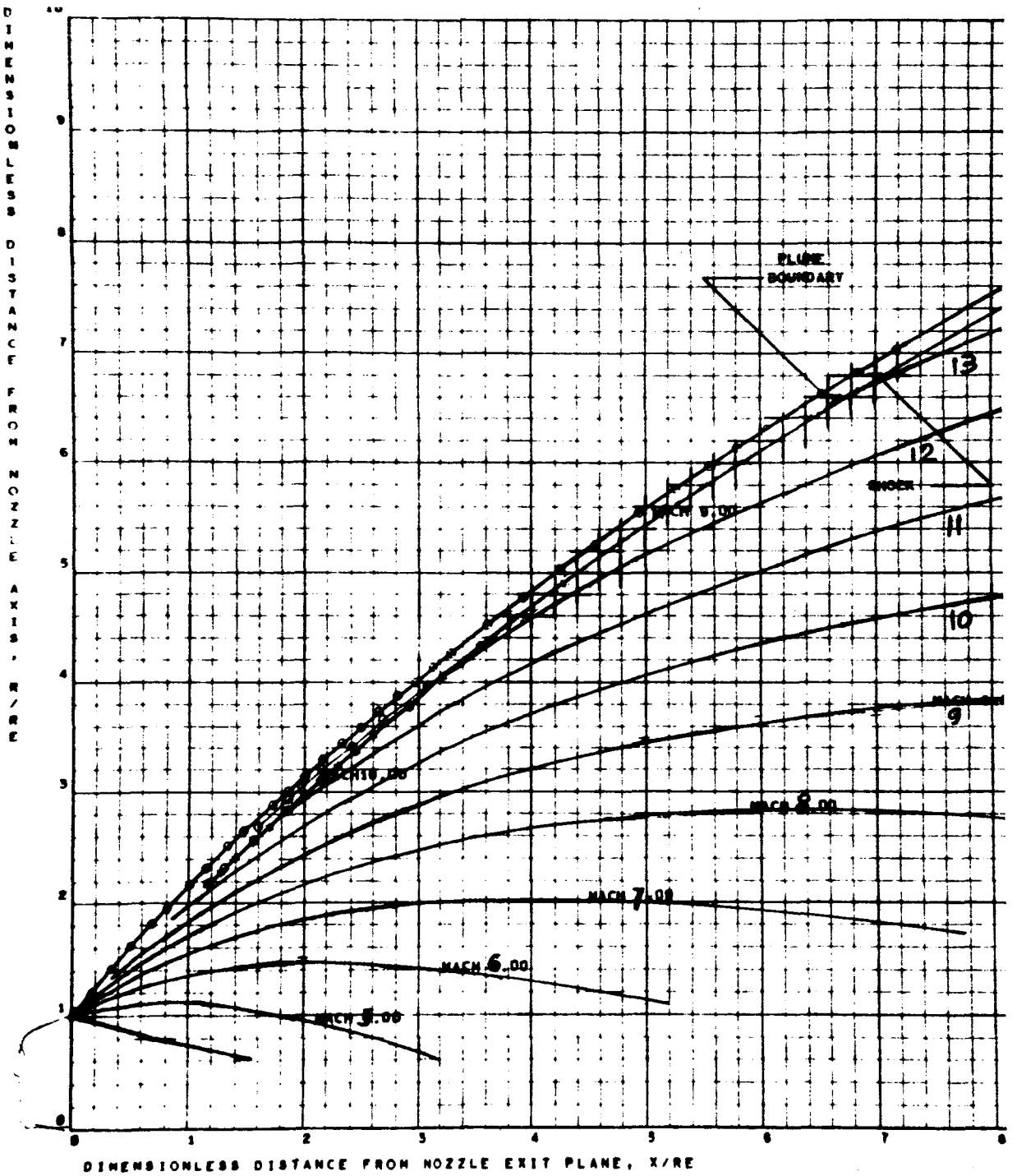

Figure 3: J-2 Engine Plume at 200,000 ft.
Equilibrium-Frozen (Freezing Point)Composition

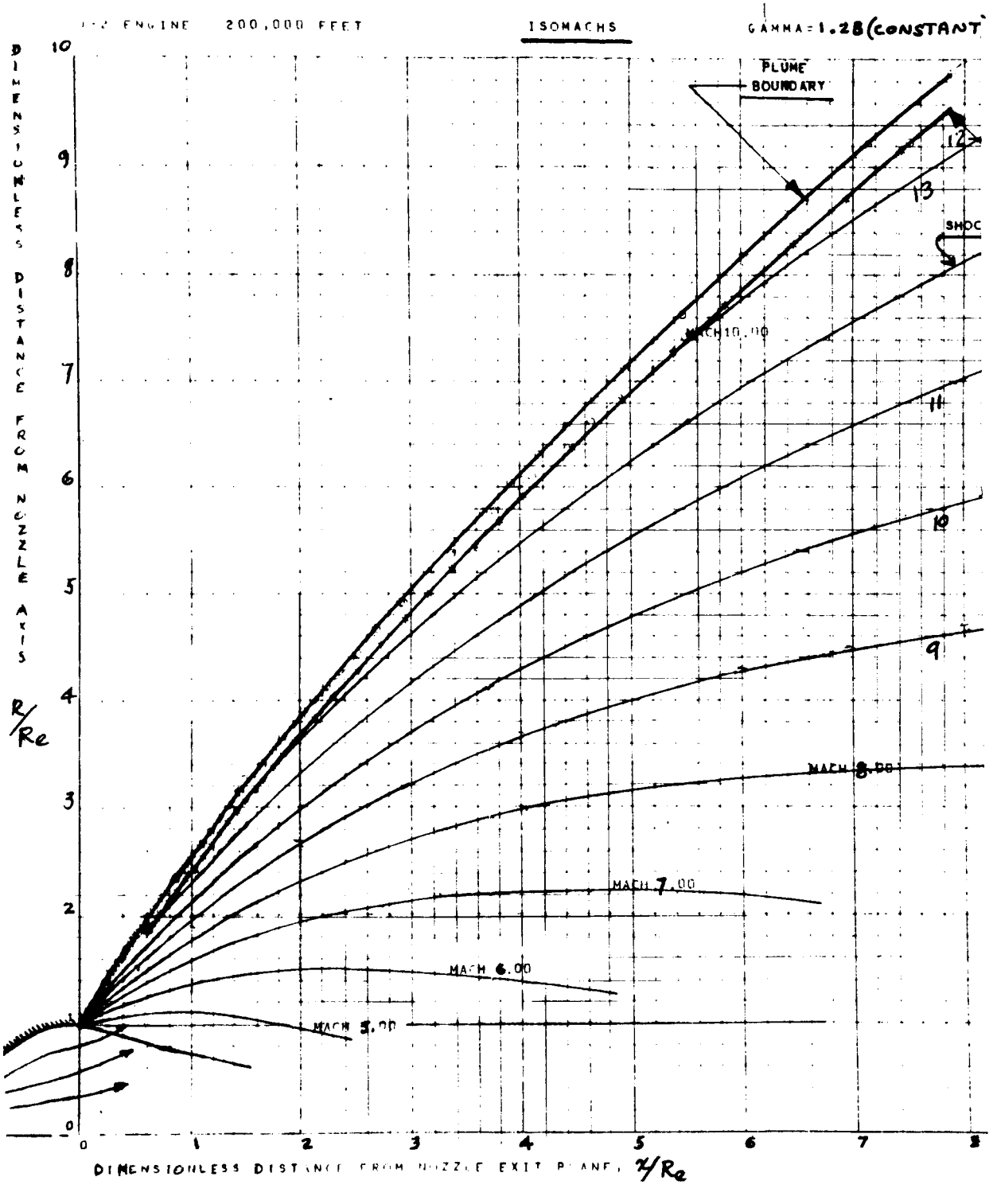

Figure 4: J-2 Engine Plume at 200,000 ft, Constant Specific Heat Ratio of 1.28

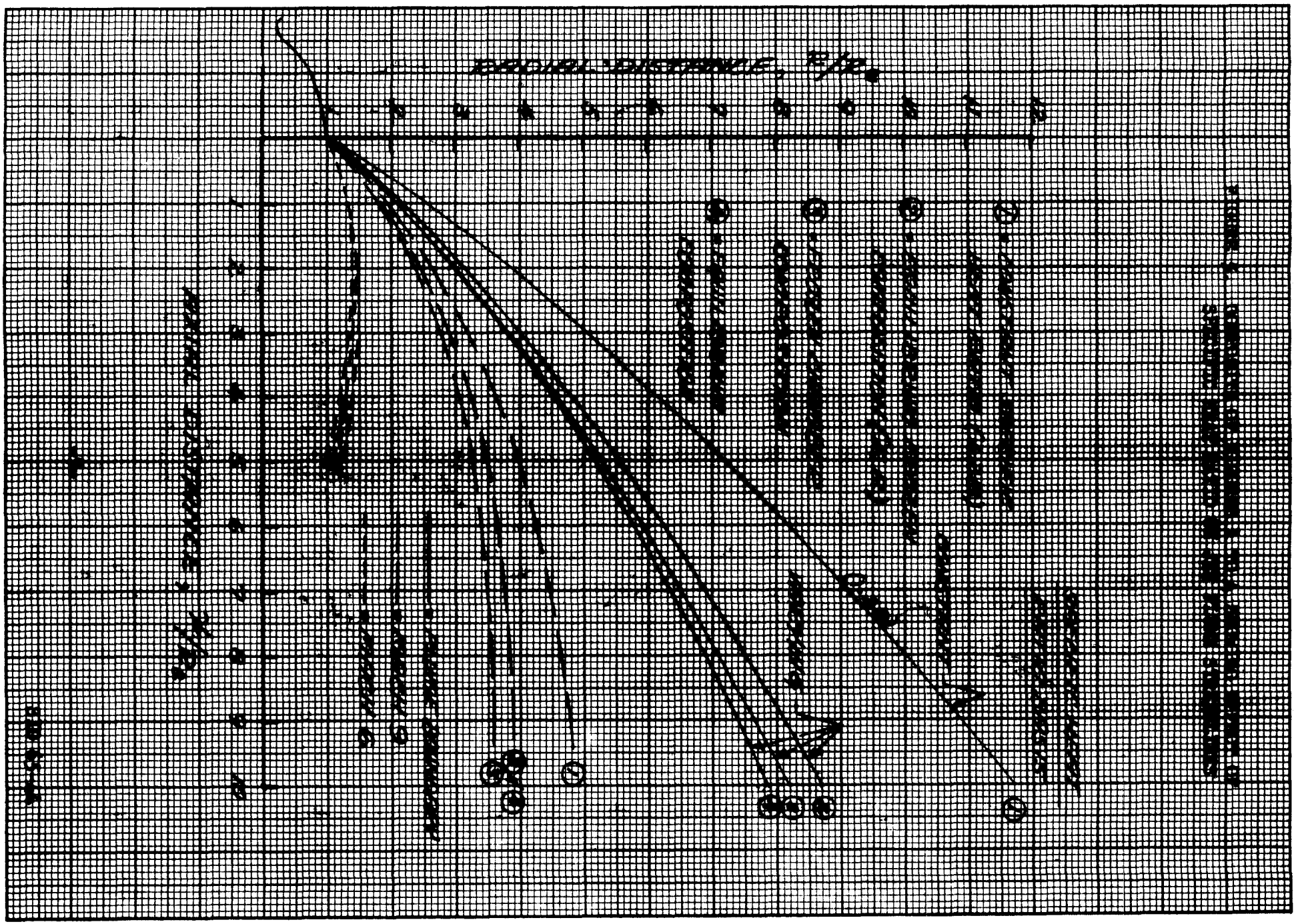

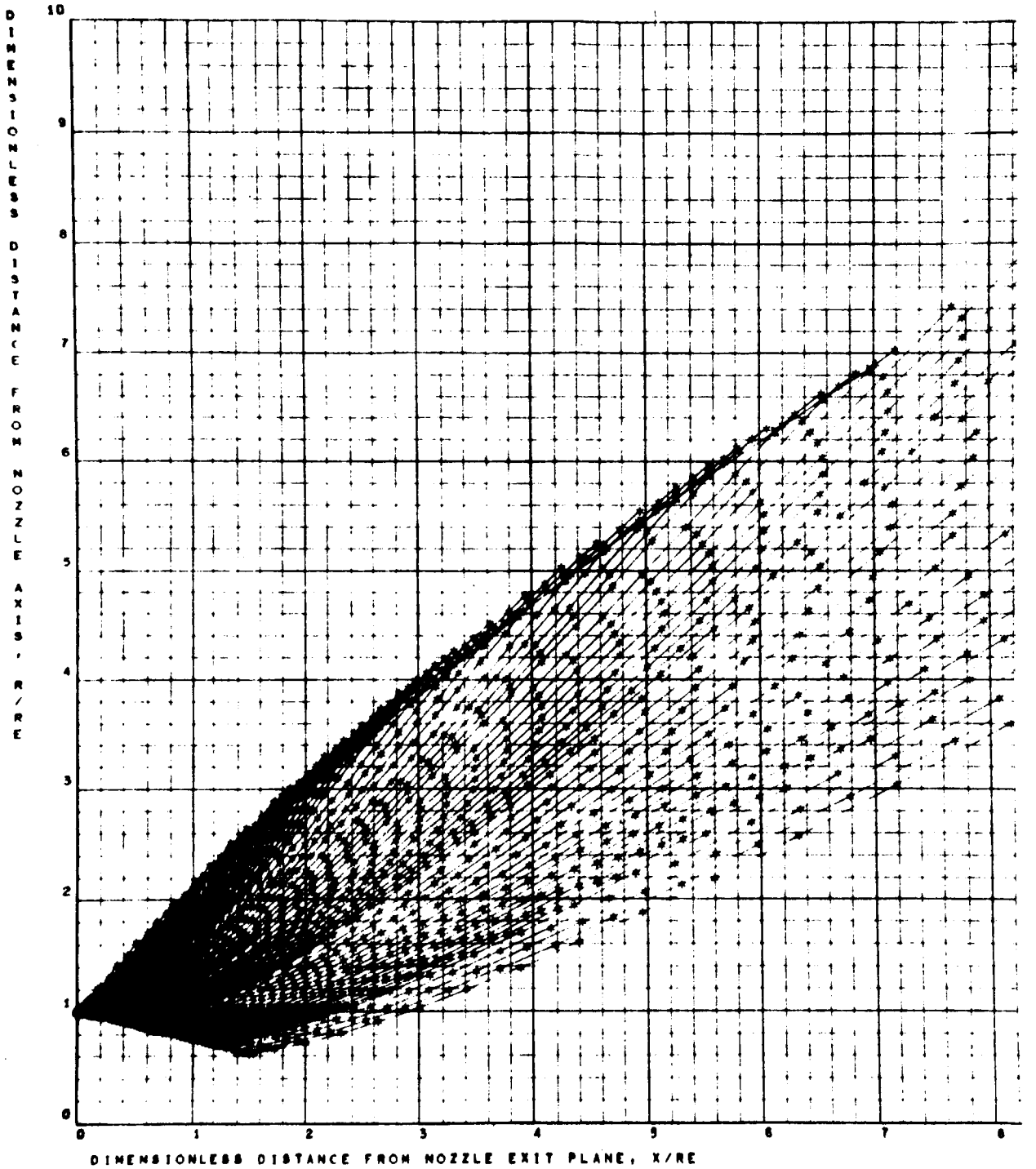

Figure 6: Showing Plume Left-Running Characteristic Lines Based on Incomplete Starting Right-Running Characteristic

III. JET PLUME INTERACTION WITH FREE STREAM

The added restriction of Newtonian impact pressures along the inviscid plume boundary was described in detail in Section IV of the First Quarterly Progress Report. During the past report period it was successfully incorporated as a subroutine in the Apollo AP 214 jet plume computer program. Figure 7 shows the marked contraction in the plume diameter for free stream Mach nos. of 5 and 10 from the original diameters of the free flow field jet plume in still air ($M_\infty = 0$). The assumed nozzle conditions were: exit Mach No. $M_e = 3.0$; constant exit and plume specific heat ratio $k = 1.3$; and exit half-cone angle $\theta_N = 15°$. A combined general nozzle/altitude condition was represented by the total nozzle exit pressure ratio to ambient pressure, $p_T/p_\infty = 10{,}000$. Cross-plots of the data in Figure 7 provided contraction ratios for this set of nozzle conditions for the intermediate freestream Mach nos. as shown in Table 1.

The marked effect of the exit Mach no. of 3 in the above case is shown by comparing the plume diameter contraction ratios at freestream Mach No. 5 with the results for an exit Mach no. of 4.

Boundary Radius Ratio	x/R_e	1	2	5	10	15
	M_e					
R_{B5}/R_{BO}	3	.56	.50	.48	.47	.45
	4	.24	.33	.40	.43	.45

It is planned to calculate similar results for a variety of conditions to attempt to generalize the trends for prediction purposes.

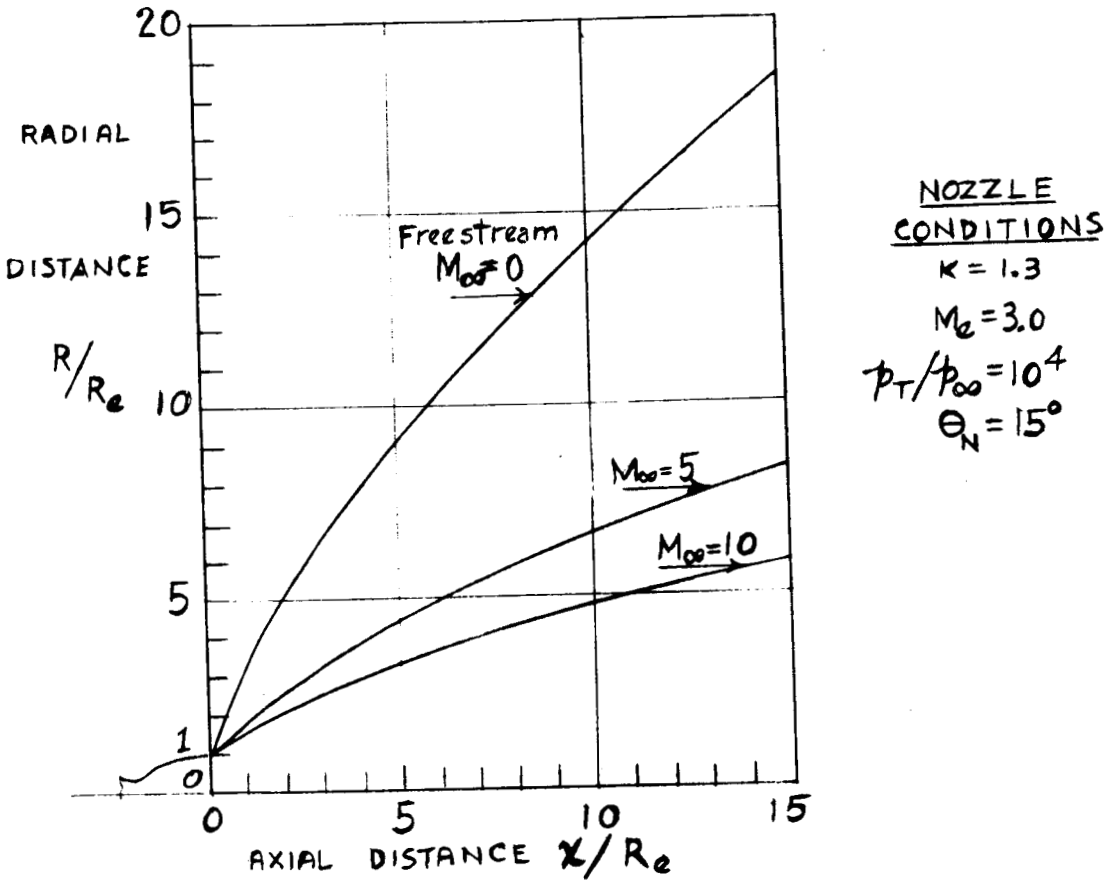

Figure 7: Effect of Freestream Mach Number on Jet Plume Boundary

Table 1

Plume Boundaries and Contraction Ratios versus Freestream Mach No. at Various Downstream Planes for $M_e = 3$; $k = 1.3$; $p_T/p_\infty = 10{,}000$, and $\theta_N = 15°$

Mach Nos. M_∞	Dimensionless Radial Distances for $x/R_e = 1$	2	5	10	15
0	3.2	5.0	9.1	14.2	18.5
1	2.8	4.1	7.0	11.0	13.8
2	2.4	3.5	6.0	9.2	11.5
3	2.2	3.1	5.3	8.1	10.1
4	2.0	2.8	4.8	7.3	9.1
5	1.8	2.5	4.4	6.6	8.3
6	1.7	2.3	4.0	6.1	7.7
7	1.6	2.2	3.8	5.7	7.2
8	1.6	2.1	3.7	5.4	6.7
9	1.6	2.1	3.5	5.1	6.3
10	1.5	2.1	3.4	4.8	5.9

Mach Nos. M_∞	Corresponding Contraction Ratios for $x/R_e = 1$	2	5	10	15
0	1.00	1.00	1.00	1.00	1.00
1	.88	.82	.77	.76	.75
2	.75	.70	.66	.65	.62
3	.69	.62	.58	.57	.54
4	..63	.56	.52	.51	.49
5	.56	.50	.48	.47	.45
6	.53	.46	.45	.43	.42
7	.52	.44	.42	.40	.39
8	.50	.42	.40	.38	.36
9	.50	.42	.38	.36	.34
10	.49	.41	.37	.33	.32

IV. APPROXIMATION OF SEA LEVEL JET PLUME PROPERTIES

Anderson and Johns mention a variety of able investigators who have attempted to develop a satisfactory theory for the mixing of a jet with quiescent air (Reference 3). The theoretical treatment is highly complex, with the decay in the supersonic region greatly complicated by shock and expansion-wave interactions.* These authors state that while significant contributions have been made, a satisfactory theoretical description of the flow in this region is practically impossible, and proceed to treat the problem from an experimental and empirical approach which yielded some very useful dimensionless pressure, temperature and velocity decay ratio profiles. Typical values of the decay ratios derived from the curves in the paper are shown in Table 2. For convenience, all five sets of ratios (A to E) are compressed in this one table to be readily available at a glance while making the empirical computations.

Table (2A) shows the impact pressure decay ratio q_{mx}/q_e, versus the dimensionless axial distance x/R_e downstream of the nozzle exit. With the nozzle exit conditions established, the basic impingement or impact pressure on a normal plane can be computed from $p_{I_e} = 2_{qe} = 2\ (\rho_e\ V_e^2/2)$. Thus, the maximum normal impingement pressure along the jet axis using the empirical decay ratios in Table (2A) is:

$$p_{I_{mx}} = p_{I_e} \frac{q_{mx}}{q_e} \qquad (1)$$

Table (2B) shows the dimensionless temperature difference ratio, $(T_{mx} - T_\infty)/(T_e - T_\infty)$ versus the axial distance, x/R_e. With nozzle exit temperature T_e and the (still) atmosphere temperature, T_∞, known, maximum temperature along the jet axis is then (with the empirical tabulated temperature difference ratio abbreviated to $r_{\Delta T}$):

$$T_{mx} = r_{\Delta T}\ T_e + (1 - r_{\Delta T})\ T_e \qquad (2)$$

* The location of the first Mach disc or Riemann shock distance was investigated. Study of the results by Love et al (Ref. 4, p. 90) indicate that no Riemann wave occurs for a nozzle exit Mach No. of about 3.2 and an exit to ambient pressure ratio of about 0.64 (values from one-dimensional flow calculation.) This appears somewhat unrealistic since a shock must occur, at least starting within the nozzle to bring the average exit pressure up to ambient pressure at or shortly downstream of the nozzle exit. Adamson (Ref. 5) emphasizes the "inability of the characteristics method solution of the jet plume to predict the first Mach disc, inherently," but describes an empirical method supported by test data for air at Me = 2. Despite the discrepancy in Mach No. his graph indicates that the shock location, if it occurs, would be very close to the nozzle exit, thus outside the path of the plume over the SA5-SA6 data points of interest.

Table 2

Typical Sea Level Decay Ratios in Supersonic and Subsonic Plumes *

(A)		(B)		(C)	
Impact Pressure Ratio q_{mx}/q	Axial Distance Ratio x/R_e	Temperature Difference Ratio $T_{mx} - T_\infty$	Axial Distance Ratio x/R_e	Axial Subsonic Velocity Ratio V_{mx}/V_s	Axial Distance Increment Ratio $\Delta x/R_e$
1.00	0	1.00	0	1.00	0
.99	5	.99	5	.90	1
.98	8	.97	10	.80	2
.95	10	.95	17	.70	4
.90	12	.90	30	.60	6
.80	15	.85	41	.50	9
.70	18	.80	53	.40	14
.60	21	.75	63	.30	20
.50	24	.70	72	.20	36
.40	28	.60	88	.10	66
.30	33	.50	101	.09	69
.20	40	.40	112	.08	77
.15	45				
.10	54				
.08	58				
.06	68				
.04	80				
.03	88				
.02	100				

* Based on empirical data, Reference (3).

(D) Half-Axial Velocity Radius	
x/R_e	R_o/R_e
10	(0.5)
15	(0.8)
20	1.0
30	1.5
40	2.0
50	2.6
60	3.2
70	3.8
80	4.5
90	5.1
100	5.8

(E)			
Radial Decay Ratios for q, V, & T	Radial Ratios		
	R/R_o for q/q_{mx}	R/R_o for V/V_{mx}	R/R_o for $\frac{T_R - T_\infty}{T_{mx} - T_\infty}$
1.00	0	0	0
.99	.15	.15	.15
.95	.24	.25	.29
.90	.32	.34	.40
.80	.45	.50	.60
.70	.57	.66	.77
.60	.70	.85	.93
.50	.75	1.00	1.12.
.40	.85	1.17	1.30
.30	1.00	1.36	1.52
.20	1.20	1.60	1.80
.10	1.45	1.95	2.15
.05	1.75	2.25	2.40
.04	1.82	2.37	2.46
.03	1.91	2.50	2.50

Table (2C) shows the empirical axial subsonic velocity ratio to the sonic velocity (Mach No. 1) at the tip of the "supersonic core or cone" versus the axial increment Δ_x/R_e, beyond the distance xs/R_e where this occurs. The supersonic cone length is estimated by assuming that the jet pressure is ambient, p_∞, and locating the axial distance xs/R_e from the critical pressure ratio

$$r_{pcr} = p_\infty / p_{total} = p_\infty / (p_{Ixs} + p_\infty) \qquad (3)$$

and its isentropic relation

$$r_{pcr} = (2/k+1)^{k/k-1} \qquad (4)$$

where k = the specific heat ratio, giving practically the same two significant-figure values for a variety of exhaust gases:

$$k = 1.23 \quad 1.26 \quad 1.30 \quad 1.4 \text{ (air)}$$

$$r_{pcr} = .56 \quad .55 \quad .55 \quad .53$$

The sonic velocity is obtained from the familiar relation

$$V_s = \sqrt{g k R_g T_{xs}} \qquad (5)$$

which raises the need for estimating the variation of the gas constant, R_g, along the axis from a consideration of the varying molecular weight. Fortunately, this is also a slow-moving variable with the asymptotic value of 29 for 100% air. The empirical axial subsonic velocity, using r_{vs} for the tabular ratio, is then

$$V_{ss} = r_{vs} V_s$$

Table (2D) shows the radial radius ratio, R_o/R_e, at which the velocity along a streamline is half of the maximum value existing along the jet axis. These values furnish the empirical distribution basis for estimating the radial decay ratios of impact pressure, velocity, and temperature difference shown in Table (2E) at particular locations in the transverse planes of the plume. For example, to find the velocity decay ratio for a point located $R/R_e = 2$ from the plume axis when the maximum velocity in the transverse plane has already been determined, first find the reference R_o/R_e value from Table (2D) at the x/R_e location, then the desired ratio can be located in Table (2E)when the listed radial ratio R/R_o satisfies the relation $(R_o/R_e)(R/R_o) = 2$. The radial impact pressure and temperature difference ratios are found in a similar manner using simple interpolation as necessary.

The approximate properties of the SA5-SA6 booster engine plume at sea level calculated in the above manner are shown in Figure 8 for use in analysis of the SA5-SA6 launch test data in succeeding sections of the present report. Some judgement was used in assuming nozzle exit conditions to account for the average overexpansion. Static pressure throughout the plume was assumed to be equal to ambient. These assumptions either proved to be near the correct values or to have little influence if incorrect since the resulting impingement pressure correlation discussed in the next section turned out to be remarkably good.

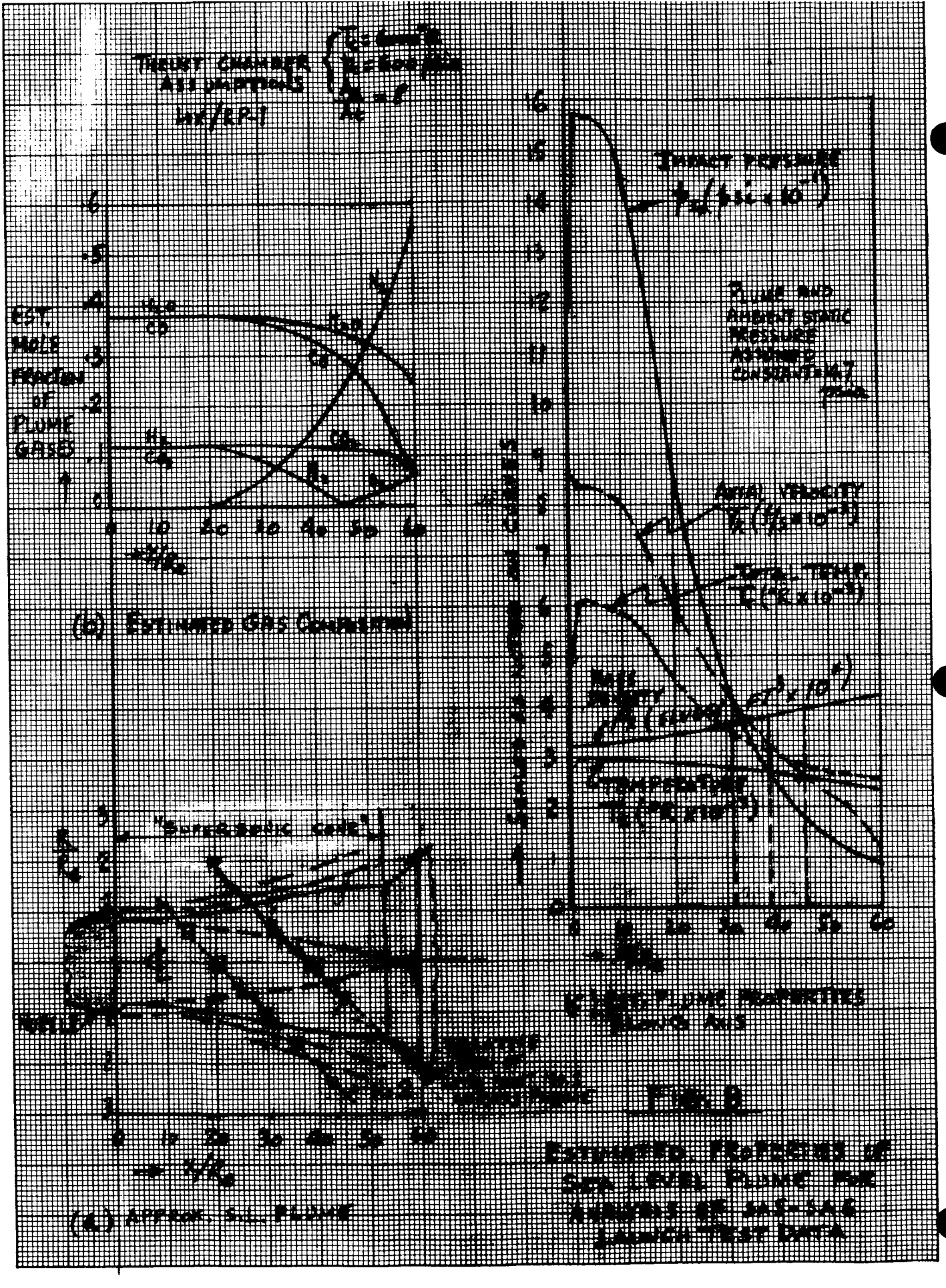

V. IMPINGEMENT PRESSURE CORRELATION

The equation based on simple Newtonian impact theory as derived in detail in the first quarterly progress report was used to compare impingement pressures versus experimental values for a variety of cases. For convenience of reference, the equation is repeated here:

$$p_{Ix} = k\, p_T \left(\frac{p_{xq}}{p_T}\right) M_x^2 \sin^2 \theta_{Ix} \qquad (7)$$

A. Apollo Plume Correlation

For the Apollo S/M RCS engines used in the high altitude chamber tests at Tullahoma, the total (average) pressure at the nozzle exit is very nearly equal to the operating chamber pressures of (83 to 101 psia) measured at the injector end. A reduction factor of 0.99 was estimated for the small effect of chamber to throat area contraction ratio. Effective gas specific heat ratios corresponding to the nozzle area expansion ratios were used together with a constant assumed chamber gas temperature of 5400°R for the storable propellants. As an example of the good correlation obtained from Equation (7), except for the peak pressure which will be discussed subsequently, the impingement pressures for the case of the cut-down nozzle with an area expansion ratio of 10, effective exit specific heat ratio of 1.28, simulated altitude pressure of about 250,000 ft (practically a space plume), and an uncanted side impingement plate located 3 exit radii from the nozzle and plume axis, are shown in Table 3 for the centerline values, and in Table 4 for the pressures along a transverse plane.

Table 3. Correlation of Impingement Pressures Along Axial Centerline

Axial Distance x/R_e	Mach No. M_x	Impinge. Angle θ_x	Impingement Pressures psia	
			Calc. Eq. (7)	Test
1	9.8	70	.05	-
2	7.5	51	.18	-
3	6.8	41	.24*	.30
4	6.6	34	.21	.24
5	6.5	29	.17	.18
8	6.9	21	.06	.07
12	7.4	15	.02	.01

*See discussion of proposed shock angle use to improve correlation.

Table 4. Correlation of Impingement Pressures, Tranverse Plane*

y/R_e	R/R_e**	θ_x	M_{xy}	Impingement Pressures psia	
				Calc. Eq. (7)	Test
0	3.0	22	6.8	.08	.08
1.1	3.2	23	6.9	.07	.07
2.0	3.6	26	7.1	.06	.06
3.3	4.5	31	7.5	.04	.05
5.5	6.2	41	8.6	.01	.02

*at $x/R_e = 7.4$
**R/R_e calculated from Eq. (12), p. 27 of Reference (1)

Following the concept of a critical shock location changing the laminar convective heat transfer from the oblique shock region to the normal shock region (Reference (1), p. 32), the hypothesis can be made that the peak impingement pressure is subject to a related interpretation of the apparent impingement angle. An apparent preliminary correlation is obtained by use of the maximum deflection angle* as a more appropriate effective impingement angle. Thus, in Table 3, for $M_x = 6.8$ and $k = 1.28$, the maximum deflection angle, from Figure 13, p. 34 of reference (1), is about 48° instead of the streamline 41°. Substituting $\sin^2 48°$ in Eq. (7) now yields 0.31 psia as the impingement pressure, which correlates well with the faired test value.

B. SA5-SA6 Plume Correlation

The approximate dimensionless distances of the two data points from the eight nozzle exit centers of the booster engine cluster were calculated from the geometry of the launch data of Reference (2) and are shown in Figure 9. Actual distances were divided by the radius of the nozzle exit, given as 3.84/2, or 1.92 ft. The corresponding dimensionless axial and radial distances with respect to the plume centerline as a function of flight time are shown in the boxed table in the same figure. The nearest engine plume is seen to be to the left of both data points Nos. 1 and 2, initially, and then sweeps over and beyond, indicating that the impingement and heat loads pass through maximum values.

Following the procedure outlined in Section IV, the plume properties are tabulated or curves plotted as in Figure 8 and used to determine local conditions at the different data point positions shown in Figure 9, with results as shown in Table 5, and plotted together with the corresponding test data in Figure 10.

* Consistent with the maximum shock angle at the same Mach number and specific heat ratio.

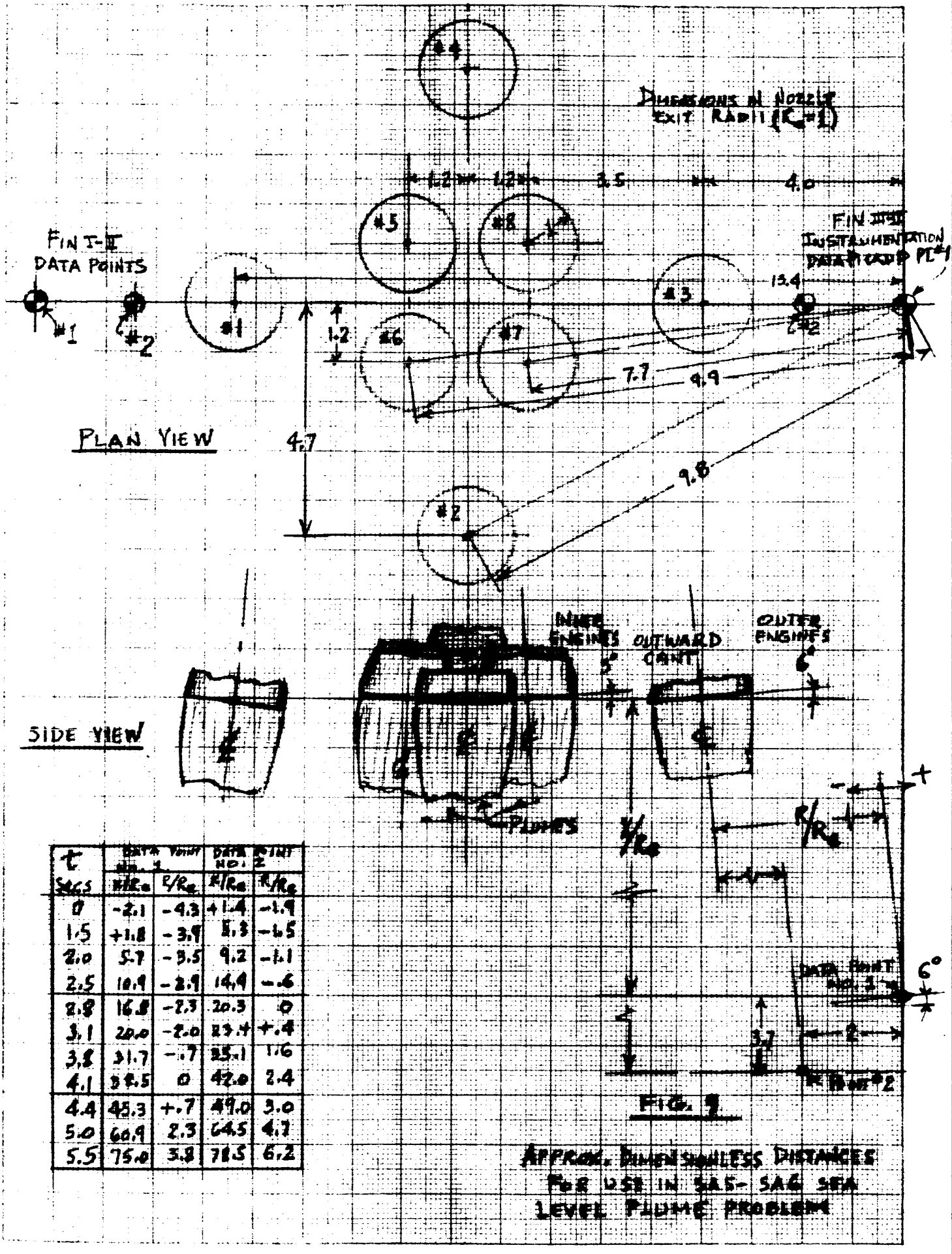

t SECS	DATA POINT NO. 1 R/R_e	DATA POINT NO. 1 R/R_e	DATA POINT NO. 2 R/R_e	DATA POINT NO. 2 R/R_e
0	-2.1	-4.3	1.4	-1.9
1.5	+1.8	-3.9	5.3	-1.5
2.0	5.7	-3.5	9.2	-1.1
2.5	10.9	-2.9	14.4	-.6
2.8	16.8	-2.3	20.3	0
3.1	20.0	-2.0	23.4	+.4
3.8	31.7	-.7	35.1	1.6
4.1	38.5	0	42.0	2.4
4.4	45.3	+.7	49.0	3.0
5.0	60.9	2.3	64.5	4.7
5.5	75.0	3.8	78.5	6.2

FIG. 9

APPROX. DIMENSIONLESS DISTANCES FOR USE IN SAS- SAG SEA LEVEL PLUME PROBLEM

Table 5. Calculation of Predicted Impingement Pressures

t, secs	x/R_e	R/R_e	p_{Imx}	R_o/R_e	R/R_o	$\frac{q_x}{q_{mx}}$	p_{IRx}	p_{Iabs}
Data Point No. 1:								
3.1	20.0	-2.0	87	1.0	2.0	0.02	1.7	16.4
3.8	31.7	-0.7	40	1.6	0.4	0.81	32.4	47.1
4.1	38.5	0.0	27	1.9	0.0	1.00	27.0	41.7
4.4	45.3	+0.7	18	2.3	0.3	0.91	16.4	31.1
Data Point No. 2:								
2.0	9.2	-1.1	151	0.5	2.2	0.00	0.0	14.7
2.5	14.4	- .6	125	0.8	0.8	0.45	56.2	70.9
2.8	20.3	0.0	85	1.0	0.0	1.00	85.0	99.7
3.1	23.4	0.4	70	1.2	0.3	0.91	63.7	78.4
3.8	35.1	1.6	32	1.8	0.9	0.37	11.8	26.5
4.1	42.0	2.4	22	2.1	1.1	0.25	5.5	20.2
4.4	49.0	3.0	15	2.6	1.2	0.20	3.0	17.7

Considering the rather approximate treatment (which is all that is justified in the application of the Table 2 statistical ratios without knowing what scaleup factors are involved) the correlation of the prediction method values with the test values is indeed remarkable. Of course, more check out of the method is in order to be sure the correlation is not fortuitous.

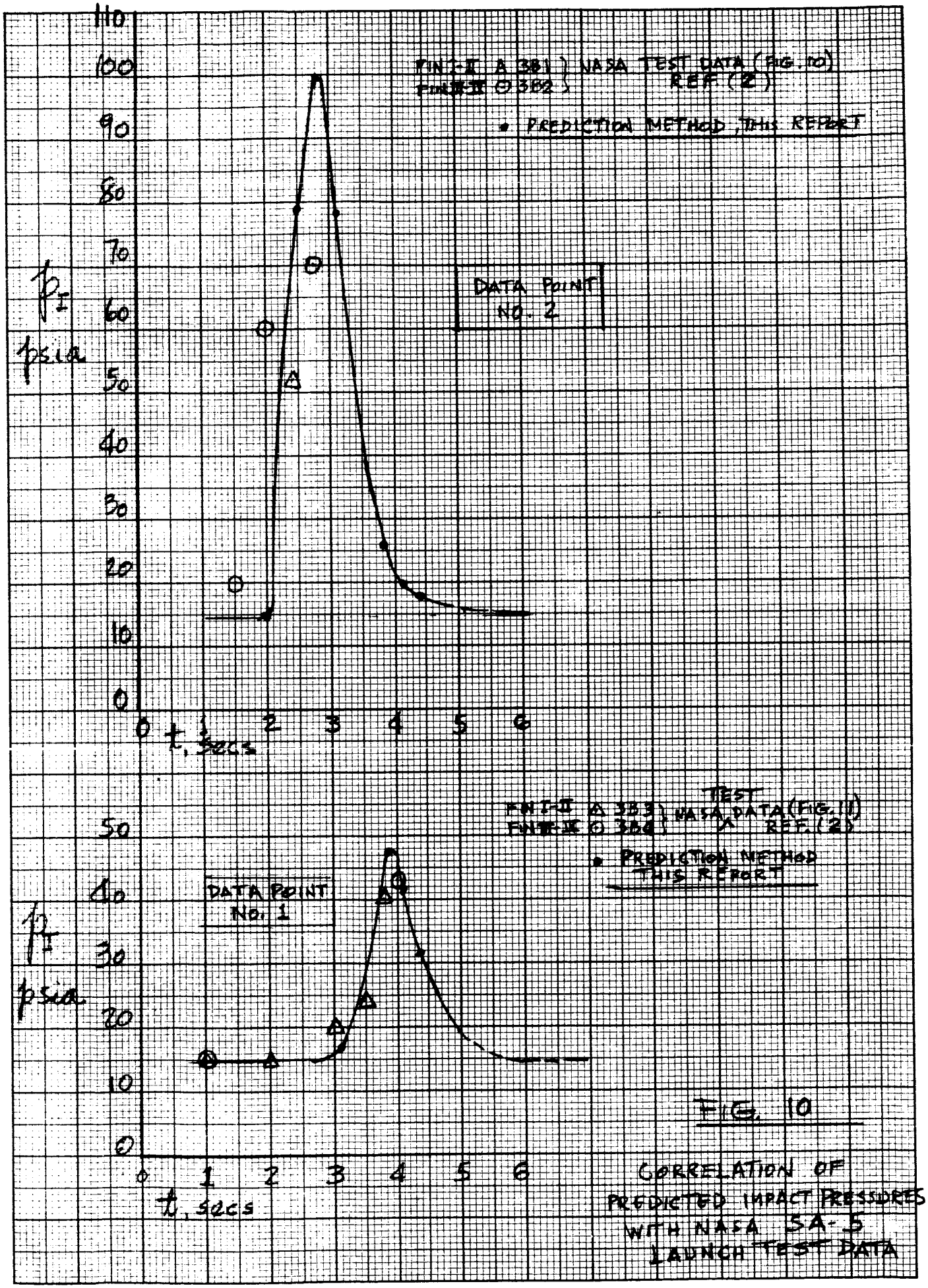

FIG. 10

CORRELATION OF PREDICTED IMPACT PRESSURES WITH NASA SA-5 LAUNCH TEST DATA

VI. CONVECTIVE HEAT TRANSFER

The method of determining the transition point between the oblique and normal shock regions of impingement on a flat plate was described in the first quarterly progress report (Reference 1), together with a discussion of the empirical equation for predicting the convective heat transfer rate in the oblique shock region. During the past quarterly report period several cases were evaluated for correlation within this region, and in addition, effort was devoted to establishing a method for computing the convective heating rate in the normal shock region and its correlation with test data.

A. Correlation Results for Oblique Shock Region

Equation (20) in Reference (1) is reproduced here for convenience in referring to the variables involved and the specific cases evaluated:

$$q_c = \frac{1.49 \times 10^{-9}}{\sqrt{X - X_{cr}}} \left(\frac{\rho_x}{\rho_{air}}\right)^{.5} U_x^{2.39} T_x^{.383} \left[1 + \frac{5}{M_x^2}\left(1 - \frac{T_w}{T_x}\right)\right] \quad (8)$$

where q_t = laminar flow convective heat transfer, BTU/ft^2 sec,

X_{cr} = axial location on the impinged plate from nozzle exit plane, where the flow changes from oblique to normal because the streamline impingement angle is greater than the maximum deflection angle for which an oblique shock can occur, ft.

X = axial location of point in the oblique shock region, ft.

ρ_X = density of gas before impingement, slugs/ft^3

$\rho_{o_{air}}$ = reference air density used in original development of equation to yield a dimensionless ratio with ρ_X.

U_x = velocity in direction parallel to plate, ft/sec.

T_x = temperature of gas before impingement, °R

T_w = wall temperature, °R

Equation (8) was used for computing the predicted convective heat transfer in the oblique shock region for several cases where experimental data were available from the Apollo S/M RCS program (Reference 6). These computations were made using theoretical values of the Mach number and impingement angle from prior results of the Apollo AP 214 plume program. The injector end combustion chamber pressure measured during the tests was assumed as the total reference chamber pressure. Comparisons of the

predicted and test heating rates shown in Table 6 and Figures 11 and 12 show good correlation in most of the axial and transverse positions.

Table 6

Correlation of Predicted and Experimental Heating Rates in the Oblique Shock Region *

Position on Side Plate		Predicted Heating Rates Btu/ft^2 Sec		Experimental Heating Rates Btu/ft^2 Sec		
Axial Z/R_e	Transverse Y/R_e					
2.4	.55	.85	.79	.75	.77	.89
2.4	1.65	.47	.54	.59	.68	
3.7	.55	1.03	1.05	1.10	1.13	1.09
3.7	1.68	.75	.69	.73	.89	.82
3.7	3.85	.17	.23	.40		
5.5	.55	1.05	1.11	1.11	1.23	1.28
5.5	1.65	.84	1.06	1.16		
5.5	3.85	.33	.35	.38		
5.5	4.95	.20	.16	.24		
7.4	.55	.86	.86	.88	.88	.94
7.4	1.65	.76	.89	.99		
7.4	2.75	.58	.64	.64		
7.4	3.85	.40	.40	.48		
7.4	4.95	.27	.30	.21		
10.6	.55	.63	.56	.59		
10.6	[illegible]	.57	.63	.67		
10.6	3.85	.38	.44	.50		
10.6	4.95	.30	.31	.35		

* For Apollo [illegible]M RCS plume: area expansion ratio $\epsilon = 40$; side [illegible]le relative to plume axis $\delta = 10°$; distance of plate from nozzle center in nozzle exit plane, $h/R_e = 3$; assumed wall temperature $T_w = 120°F$.

B. Theoretical Prediction Equation for Normal Shock Region

An empirical equation giving the convective heat transfer in the normal shock region from the known upstream plume properties and developed in prior NAA/S&ID Apollo work in this area (Reference 7) is:

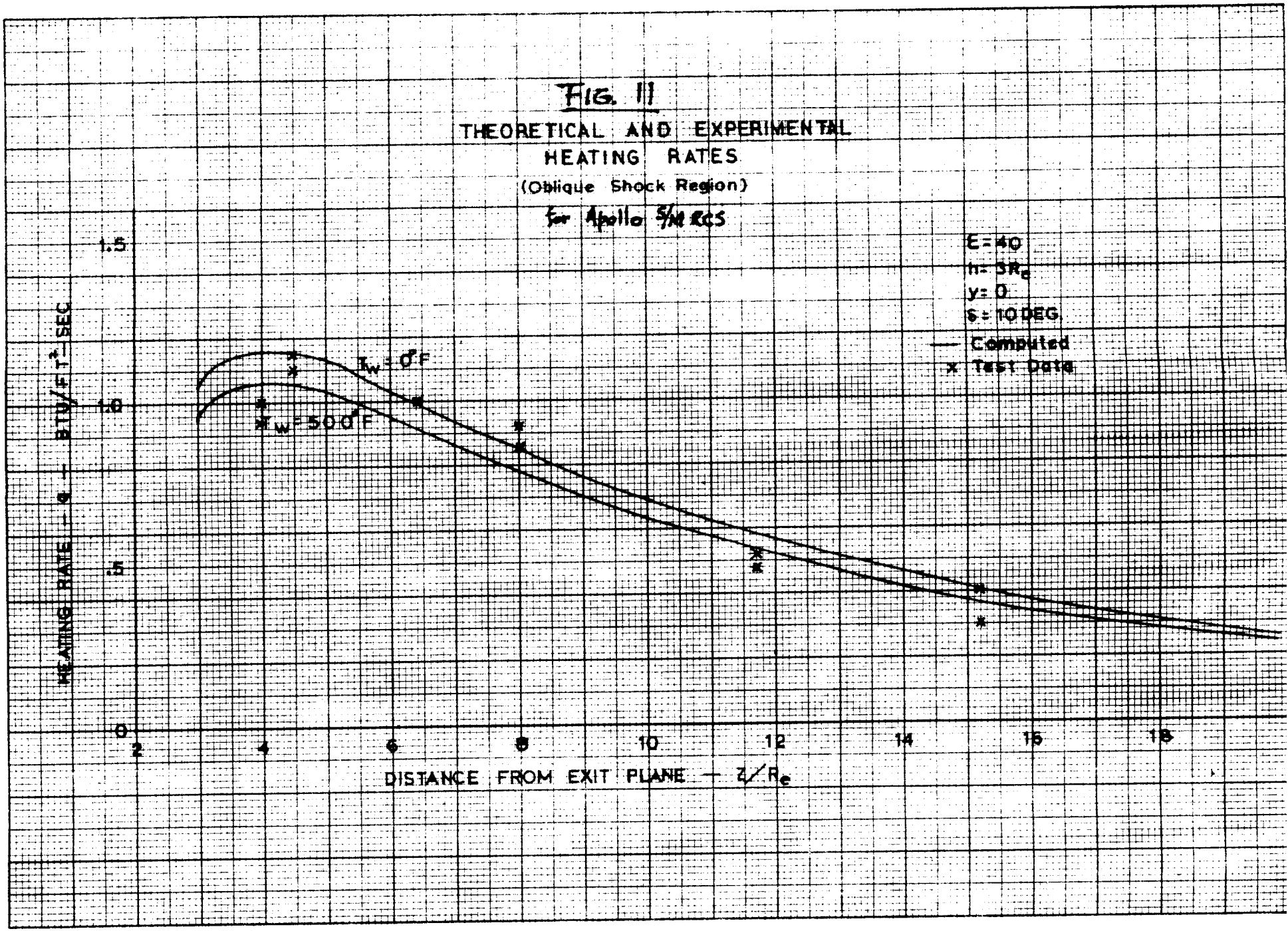
FIG. 11
THEORETICAL AND EXPERIMENTAL
HEATING RATES
(Oblique Shock Region)
for Apollo S/M RCS
E = 40
h = 3Re
y = 0
δ = 10 DEG.
— Computed
x Test Data
Tw = 0°F
Tw = 500°F
HEATING RATE — q — BTU/FT²-SEC
1.5
1.0
.5
0
2
4
6
8
10
12
14
15
16
DISTANCE FROM EXIT PLANE — Z/Re

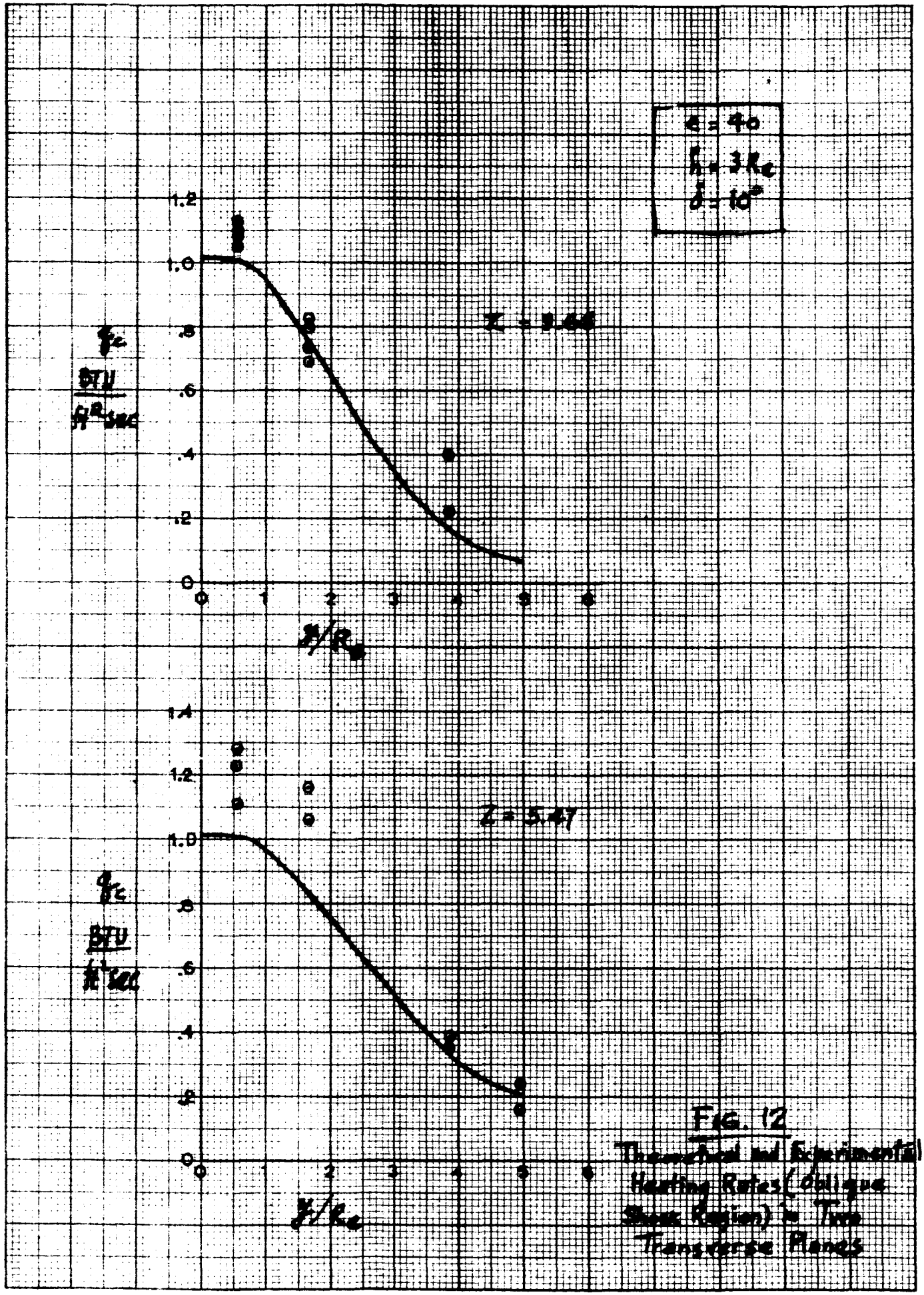

FIG. 12
Theoretical and Experimental Heating Rates (Oblique Shock Region) in Two Transverse Planes

$$q_c = \frac{15200}{\epsilon + 0.75\, h/R_e} \left(\frac{\rho}{\rho_{SL}}\right)^{.5} \left(\frac{V}{V_m}\right)^{3.25} \left(1 - \frac{H_w}{H}\right) \quad (9)$$

where

q_c = convective heat transfer for normal shock, Btu/ft^2 sec.

ϵ = nozzle area expansion ratio

h/R_e = dimensionless distance in the nozzle exit plane from center of nozzle to the impinged side plate

ρ/ρ_{SL} = ratio of gas density before impingement to that of standard air at sea level

V/V_m = ratio of gas velocity before impingement to maximum velocity in a vacuum, and

H_w/H = ratio of gas boundary layer enthalpy at the wall to total enthalpy.

This equation was adapted from the Kemp and Riddell empirical satellite reentry heating equation (Reference 8), keeping the basic form, but replacing the value of the original constant (20,800) by 15,200 and the square root of the nose radius ($\sqrt{R}$) in the denominator by the expression $\epsilon + 0.75\ h/R_e$ to relate the equation empirically to the engine and test configuration.

The reciprocal of the square root of the reference air density is, of course, a constant which can be combined with the 15,200 to give 55,000 as the numerical coefficient. Also, the theoretical ratio of rocket exhaust velocity to its maximum under fully expanded conditions in a vacuum is simply the square root of the ratio of the nozzle expansion efficiencies $\sqrt{\eta/1} = \sqrt{1 - T_x/T_c}$. Finally, if the specific heat is assumed nearly constant, the ratio of local wall to stagnation enthalpy can be approximated by the temperature ratio T_w/T_t giving the simplified relation:

$$q_c = \frac{55000}{\epsilon + 0.75\ h/R_e} (\rho x)^{.5} \left(1 - \frac{T_x}{T_t}\right)^{1.625} \left(1 - \frac{T_w}{T_t}\right) \quad (10)$$

Further modifications are desirable to make the relation dependent only on the impingement gas velocity or Mach number, density, and orientation. However, to permit the Phase II correlation effort to proceed on schedule, the form of Equation (9) or (10) was used. Upstream Mach nos. streamline orientations, and constant nozzle exit specific heat ratio obtained from prior Apollo characteristics solution of jet plume free flow fields were used, together with the estimated nozzle exit conditions and density and temperature ratios from the gas tables for isentropic expansion to evaluate this equation.

Comparison of the predicted and experimental convective heat transfer rates for this normal shock region are shown in Table 7 for various positions on a side plate parallel to the nozzle axis and for two area expansion ratios and wall separation positions. Again, the correlation appears to be good.

Table 7

Correlation of Predicted and Experimental Heating Rates in the Normal Shock Region*

Expansion Ratio ϵ	Separation h/R_e	Distance Z/R_e	Wall Temp** °F	Heating Rates Btu/ft^2-sec	
				Computed	Measured**
10	7	3.9	0	3.55	3.6
			500	3.23	
		6.1	0	5.4	4.2
			500	4.85	
	5	1.2	0	2.05	2.9
			500	2.35	
		3.7	0	7.3	8.2
			500	6.6	
15	7	5	120	2.55	2.1,2.4
	5	3	120	3.1	3.45,3.75

* For Apollo S/M RCS Plume (Cant angle $\delta = 0$ giving $Z/R_e = x/R_e$)

** Applies to computed heating rates only; wall temp. for measured heating rate between 70 and 200°F.

C. Correlation of SA5 Thermal Data

As of this writing, the convection heat transfer equation which has been used successfully to correlate predicted values with the Apollo high-altitude test data in the normal shock region, has not yielded a similarly good correlation with the Reference (2) data from the SA5 launch. The predicted heat transfer values appear to be low. The radiation heat transfer rate is not yet available, but is not expected to be large enough to pick up the discrepancy.

The discrepancy in results could be attributed to various causes: (1) the numerical coefficient in Equation (8) may be too low because the original aerodynamic test data may not have included the effects of radiation heating at high enough temperatures (which would not affect the correlation obtained for the highly expanded gases of the Apollo RCS); (2) the expression used in the denominator may not fit sea level plume data; (3) unlike the test impact pressures, the measured heat transfer rates indicate excessive scatter in both peak levels and times. A small $\pm$ 1 degree of gimbaling could account for some of the apparently incorrect times, since a calculation of the sweep of the plume at a distance of $(100 + x)/R_e$ indicates a possible radial shift of about $\pm$ 1 exit radius and about one second in equivalent liftoff time.

Additional data from other launches would be useful to add confidence to the results of the analysis. This effort will be continued using the estimated radiation rates when they become available, and reported in later progress reports.

VII. PLUME RADIATION STUDY

A. Introduction

The previous quarterly report (Reference (1)) described a general method of predicting total radiant power from an exhaust plume containing only molecular radiations. The detailed numerical example presented there applied to a high altitude or near-vacuum plume but the method is applicable to any axisymmetric plume whose temperature, density, and composition distributions can be specified.

This report contains the results of the remaining analytical work accomplished on plume radiation. This includes molecular radiation from low altitude plumes and the new topic of radiation from particle-laden plumes.

B. Molecular Radiation from Low Altitude Plumes

At high altitudes and in space the exhaust plume may be considered isentropic and non-reacting. Hence composition can be assumed constant and temperature and pressure may be simply computed from the local Mach number. Moreover, the Mach number can often be represented by a simple analytical function of axial and radial location (see Equation (41), Reference (1)), thus yielding a fairly compact representation of plume properties.

At low altitudes, these simplications are no longer valid. The core of the plume will, in general, contain a series of expansion and compression shocks across which gas properties change discontinuously. Moreover, there may be large composition changes due to reaction between the fuel-rich exhaust and the entrained atmosphere ("after-burning").

Instead of the relatively simple analytical expressions applicable to high altitude plumes, therefore, the more general expressions must be used.

$$T = T(X,R) \tag{11}$$
$$P = P(X,R) \tag{12}$$
$$N = N(X,R) \tag{13}$$

In machine computation, Equations (11), (12), and (13) would be represented by tabulated data with associated interpolation subroutines. In principle, however, the calculation of absorption coefficients proceeds exactly as in the case of the high altitude plume. The real difficulty is encountered in specifying the functions T, P, and N. As pointed out in Section IV of this study, there appears to be no method analogous to the method of characteristics by which the properties in a low altitude plume can be calculated accurately. In the numerical example, given in a later section, rather rough assumptions of properties are made in order to arrive at an approximate

estimate of radiation heating during launch.

C. Plume Geometrical Relationships

In order to evaluate the radiant intensity reaching a surface element from a given direction, it is convenient to work with the two coordinate systems shown in Figure 13. The integration of the equation of radiative transfer through the plume is carried out along lines of sight whose orientation is specified with respect to a reference plane defined by the position of the surface element, P, and the plume axis (Figure 13A). Direction is given in terms of an azimuth angle, θ, measured from the rearward axial direction in the reference plane and an elevation angle Φmeasured perpendicular to the reference plane. Distance, S, along the line of sight defines a particular location in the plume.

The same system is used to define the orientation of the surface element at point, P, in terms of the directional coordinates, θ_r and Φ_r of its normal.

The temperature, pressure, and composition of the plume from which the radiative characteristics of the plume are determined, are most conveniently described in terms of X and R, the axial and radial coordinates depicted in Figure 13B. These are related to the previously-described coordinates by

$$X = Y + S \cos \Phi \cos \theta \tag{14}$$

$$R = S^2 \sin^2 \Phi + R_o^2 - 2R_o S \cos \Phi \sin \theta + S^2 \cos^2 \Phi \sin^2 \theta \tag{15}$$

Unfortunately, a geometrical error was made in the derivation of Equation 40 in the previous quarterly progress report (Reference 1). Equation 40, which gives the radiant power per unit area reaching a surface element, contains the factor $\cos (\Phi - \Phi_r) \cos (\Phi - \Phi_r)$ which was intended to correct for non-normal incidence. This factor is corrent when either the surface normal or the line of sight cross the plume axis (Φ_r or $\Phi = 0$) but becomes increasingly in error as both Φ_r and Φ approach 90°. The correct form of Equation 40 is

$$P = \iiint \left[\sin \phi_r \sin \phi + \cos \phi_r \cos (\theta - \theta_r) \right] \left[\int_o^\infty I_\nu \, d\nu \right] \cos \phi \, d\phi \, d\theta \tag{16}$$

This error will affect the numerical results presented in Reference 1, but will probably be significant only for surface elements located within a few radii of the plume. There has not been sufficient time to recheck the previous calculations and to include the results in this report, but this will be reported on later.

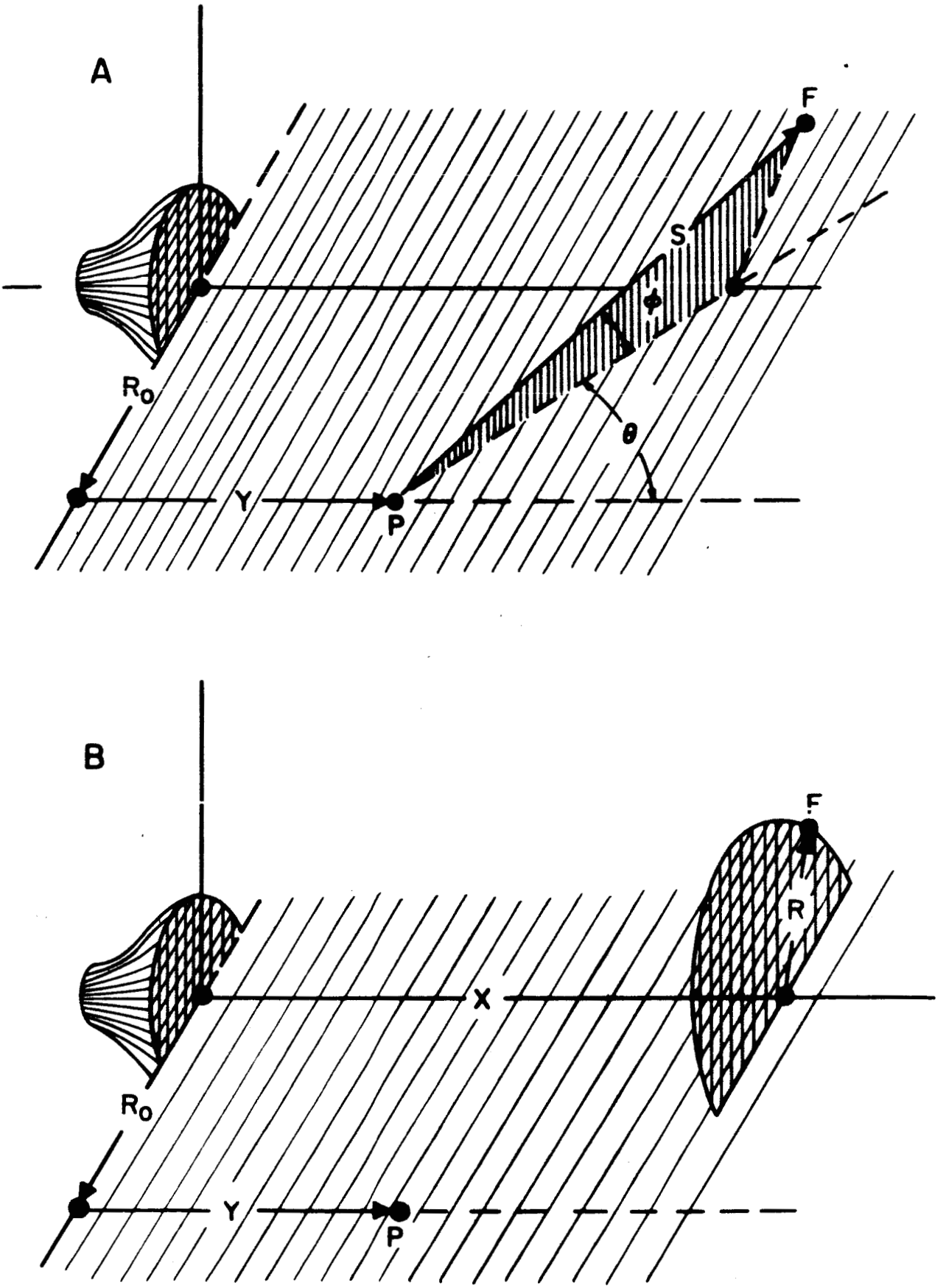

Fig 13 Plume Coordinate Systems for Radiation

D. Radiation from Particle-Laden Plumes

In spite of the fact that radiation from particles generally has a simpler spectral dependence than that from molecular radiators, the overall problem of evaluating the contribution due to solid (or liquid) particles in an exhaust plume is very difficult. First, the radiative characteristics of individual particles must be determined as a function of wavelength and of particle size and temperature. Next, the net effect of a cloud of such particles (not necessarily uniform in size, concentration, or temperature) must be evaluated, considering both absorption and scattering of radiation. Finally, and perhaps the most difficult, the actual particle size distribution, concentration and temperature must be predicted as functions of plume location for a given rocket engine. The principal solid or liquid constituents in rocket plumes are carbon, resulting from the incomplete combustion of hydrocarbons, and the oxides of aluminum and magnesium which are equilibrium products for many solid propellants.

E. Cross Sections for Carbon Particles

Stull and Plass (Reference 9) have computed the absorption, scattering, and total cross sections of spherical carbon particles, using Mie scattering theory. They considered particle radii from 50 to 1000 Å the expected range for carbon particles in flames according to their review of available measurements. Although the expressions for cross sections are quite complex, the resulting values can be represented fairly simply for wavelengths which are large compared to particle radius. Fortunately this covers the spectral region from which most of the radiant energy is emitted at typical plume temperatures. The cross sections are

$$\sigma_s = 1.12 \times 10^{-4} \, r^6 \, \lambda^{-4} \tag{16}$$

$$\sigma_t \approx \sigma_a = 6.05 \times 10^{-7} \, r^3 \, \lambda^{-2} \tag{17}$$

The cross sections are in square centimeters, and radius and wavelength are in microns.

In the range where they apply ($r < 0.1\ \mu$, $\lambda > 1.0\ \mu$), Equations 16 and 17 have two important consequences: First, absorption is the dominant extinction mechanism and scattering can be ignored for most engineering purposes. Secondly, the product $N \sigma_t$, where N is the volume concentration of particles in a cloud, is proportional to $N r^3$ and thus to the mass density of particles. Thus $N \sigma_t$, which is essentially a volume absorption coefficient, is independent of particle size and size distribution.

F. Cross Sections and Emmisivities of Oxide Particles

The aluminum and magnesium oxide particles observed in solid propellant exhausts range in size from less than a micron to several microns in radius (see References 10, 11, 12). Thus the spectral variation of radiation cross sections is more complicated than for the much smaller carbon particles. Typically the total or extinction coefficient, σ_t, at a given wavelength increases monotonically with particle radius r_p, for particles small compared with the wavelength. For particles having radii greater than about one-third wavelength σ_t oscillates about the value $2\pi r_p^2$, finally damping out at large radii. Reference 11 gives total and absorption cross sections for Al_2O_3 and MgO particles over a range of sizes and wavelengths.

Morizumi and Carpenter (Reference 10) inltheir analysis simplify this complicated behavior by assuming the constant asymptotic value $2\pi r_p^2$ for the extinction coefficient. This represents a rough average to the actual values for particles in the micron range and is probably a reasonable choice since particle size and size distribution are not accurately known.

Current knowledge of Al_2O_3 and MgO particle emissivities, which can be derived from the absorption and total cross sections, is uncertain at present. Typical values derived from the cross sections computed by Plass (Reference 11) are less than 0.1 but later work by the same laboratory (Reference 12) indicates that these values are too low for particles at plume temperatures and that emissivities probably lie in the range 0.2 to 0.4. In Reference 10, the value 0.25 is adopted, based upon an analysis of radiation from actual rocket exhausts.

G. Gas-Particle Nozzle Flow

There have been a number of numerical studies of the behavior of two-phase flow in rocket nozzles and isentropic plumes. The results of such calculations are presented in References 10, 13, and 14. In general the velocity and temperature history of the particles are computed from the drag and heat transfer exerted by the gas stream.

In all the references cited, the calculations are based upon the assumption of spherical particles. Drag and heat transfer are evaluated in the flow regime where viscous behavior predominates (Stokes flow). References 10 and 13 include corrections for rarefaction effects. Reference 14 also takes rarefaction into account and in addition employs corrections for compressibility and inertial effects which can be important for large particles and large relative velocities.

No similar computer program is available at the Space and Information Systems Division of North American Aviation and it is not within

the scope of the present study to develop one. As an alternative, the numerical results of detailed calculations have been correlated to provide engineering expressions useful for the estimation of the radiative properties of gas-particle clouds.

H. Velocity Lag Correlation

In general, the axial velocity of a particle will lag the velocity of the gas stream during acceleration through the nozzle and in the external plume. The amount of this lag depends upon nozzle shape and size, particle size and density, and gas properties. Since carbon particles are found to be very small, only Al_2O_3 and M_gO particles in the micron range are likely to exhibit appreciable velocity lag. The densities of the latter two are fairly close so that, in practice, only particle size need be considered. Again, it is reasonable to expect that nozzle contours and gas composition and temperature variation through the nozzle will be similar for modern solid propellant rockets. Thus, as an approximation, the significant variables are nozzle scale and axial distance along the nozzle.

The velocity lag (1-k, where $k \equiv V_p/V_g$) can be successfully correlated with the parameter $r_p(r^*)^{-\frac{1}{2}}Z^{\frac{1}{4}}$ where r_p, r^* and Z represent the particle radius in microns, the nozzle throat radius in centimeters, and the axial distance downstream of the throat in centimeters, respectively. This correlation is shown in Figure 14. As may be seen, there is considerable difference between the curve which includes corrections for inertial and compressibility effects and that which includes only rarefaction effects.

I. Temperature Lag Correlation

An examination of the numerical predictions for particle temperature lag $(T_p - T_g)/T_{go} - T_g)$, where T_{go} is the gas temperature in the combustion chamber, shows that lag reaches an asymptotic value within the diverging portion of the nozzle and remains essentially constant thereafter. Thus, the value of the temperature lag at the nozzle exit is apparently not sensitive to nozzle length. In fact, a reasonable satisfactory correlation of the data from References 13 and 14 can be made using particle radius alone (see Figure 15).

Unlike the situation with the velocity lag, there is no consistent trend identified with the consideration of inertial and compressibility effects. It should be noted that the apparent lack of influence of nozzle scale is based on the data used in Figure 15 which covers nozzle radii from 1.5 to 3.5 centimeters. For much larger nozzles, the temperature lag at the exit must certainly be less than the correlation indicates.

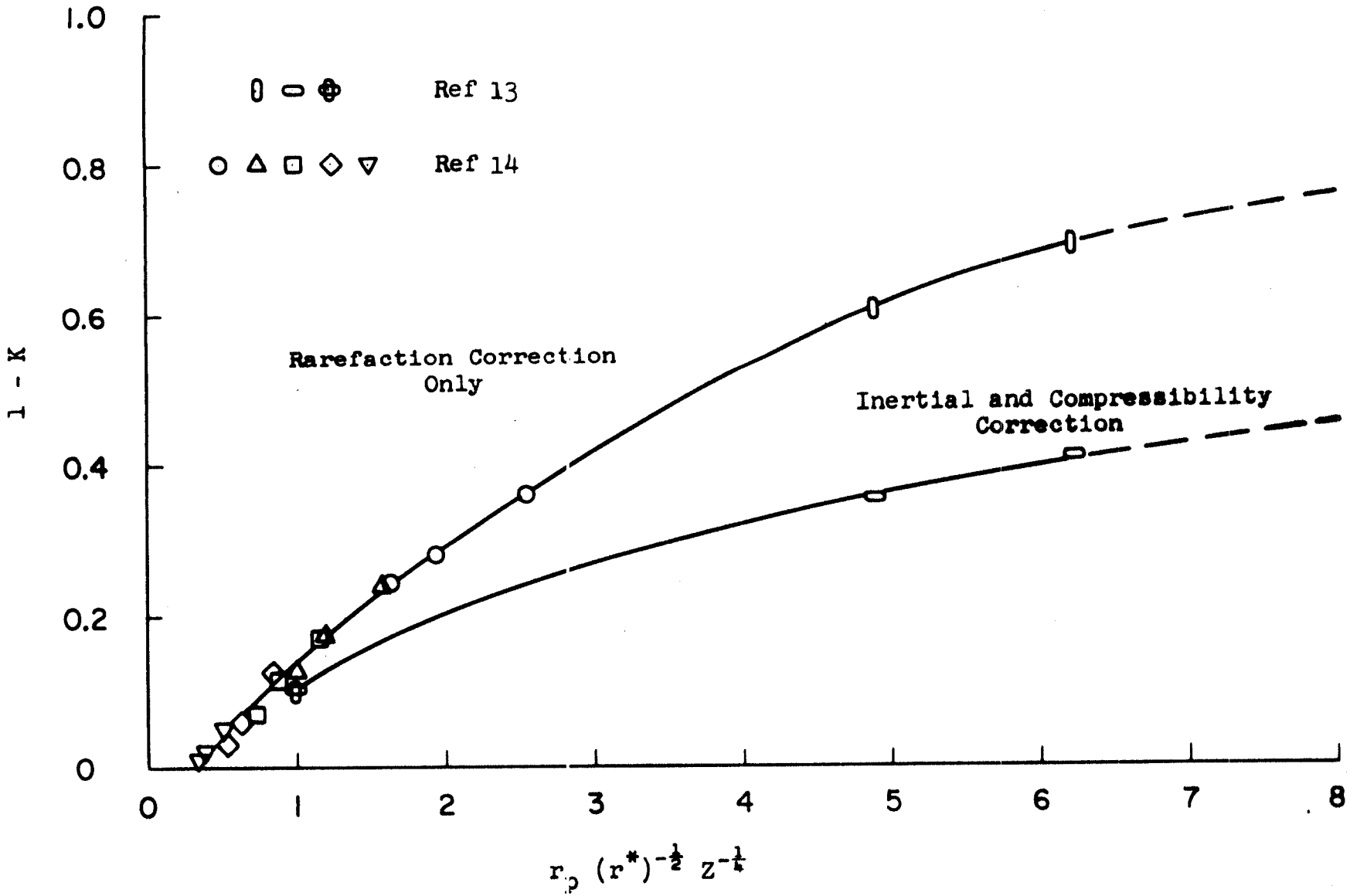

Fig 14 Velocity Lag Correlation

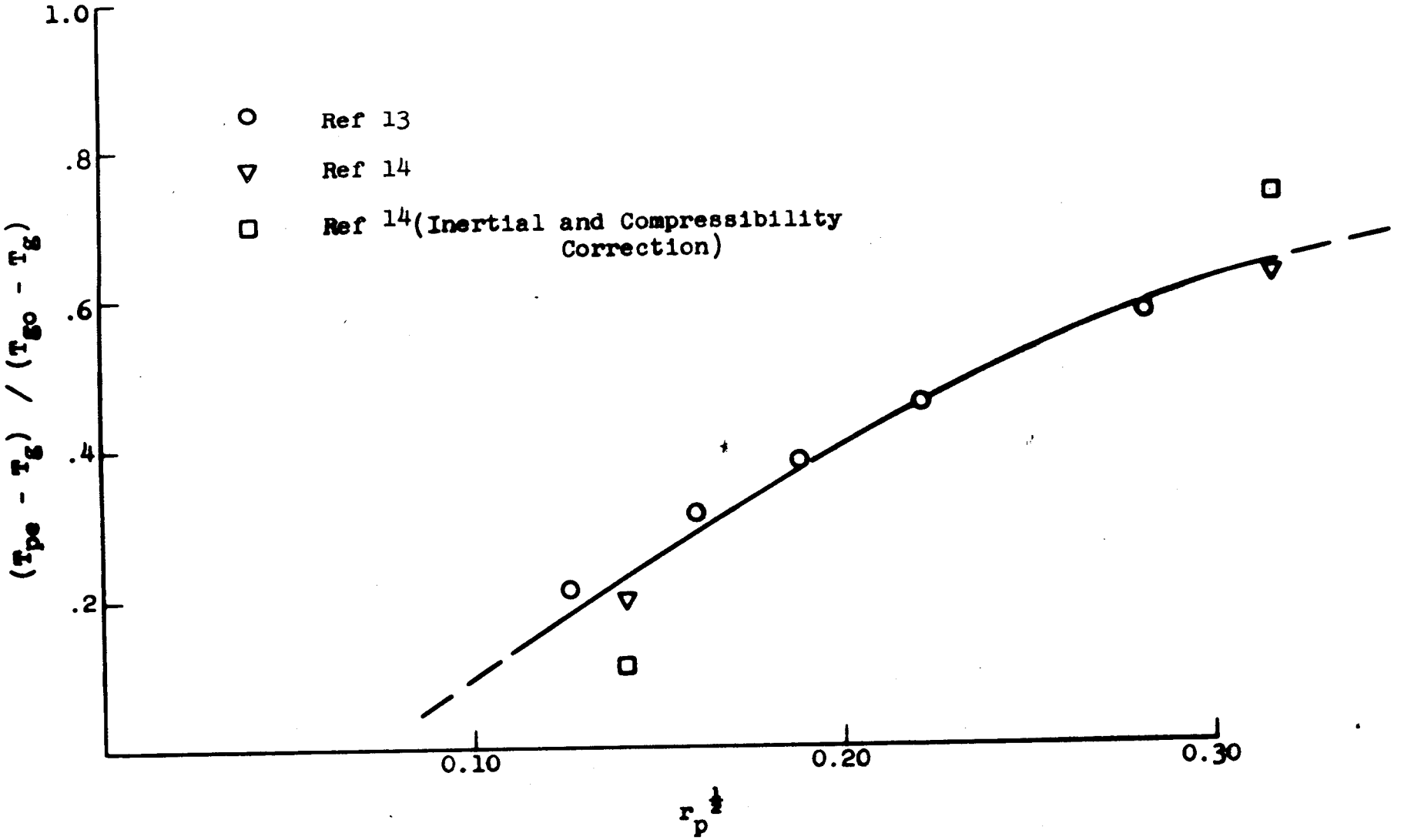

Fig 15 Temperature Lag Correlation

J. Particle Concentration Correlation

As Kliegel (Reference 13) points out, particles tend to travel in straight lines in the diverging portion of the exit nozzle and in the plume, and in fact exhibit conical flow regardless of nozzle contour. This observation is used as the basis for an approximate method of specifying particle concentrations in the plume.

Assume that particles in the plume are confined to a cone centered on the nozzle axis whose apex is at the nozzle throat and whose half angle θ_L is determined by the limiting streamline for a particular size. Assume further that the particle concentration N_p is constant in magnitude and directed along streamlines perpendicular to the apex. Under these circumstances the particle mass flow $\dot{M}_p$ through any surface X = constant becomes

$$\dot{M}_p = 4/3\ \pi\ r_p^3\ \rho_p\ N_p\ V_p\ A\ (X) \tag{18}$$

The area A (X) becomes

$$A\ (X) = 2\ \pi\ X^2\ (1 - \text{Cos}\ \theta_L)$$
$$\approx \pi Z^2\ \theta_L^2,\ (\theta_L \text{ small})$$

The particle concentration may now be expressed

$$N_p = \frac{M_p}{4/3\ \pi \rho_p\ V_g} \quad \frac{1}{r_p^3\ K Z^2\ \theta_L^2} \tag{19}$$

The term in brackets depends upon the particle size and nozzle geometry. The particle velocity may be taken as the value at the nozzle exit and is obtainable from the gas exit velocity through Figure 14. The limiting streamline angle θ_L may also be correlated with particle size as shown in Figure 16. θ_L varies inversely with the square root of the particle radius until it exceeds the nozzle half angle, after which it remains roughly constant.

No published calculations of plume particle concentrations have been found in which enough information is included to allow a direct test of Equation 19. However Reference 10 presents calculated concentration distributions for two particle sizes, 0.79 and 3.95 μ, which are assumed to have equal mass fractions in the exit flow. Thus the term outside the bracket in Equation 19 is constant, and N should vary inversely with $r_p^3\ K\ Z^2\ \theta_L^2$. Figure 17 shows that the calculated concentrations do obey this relation fairly closely.

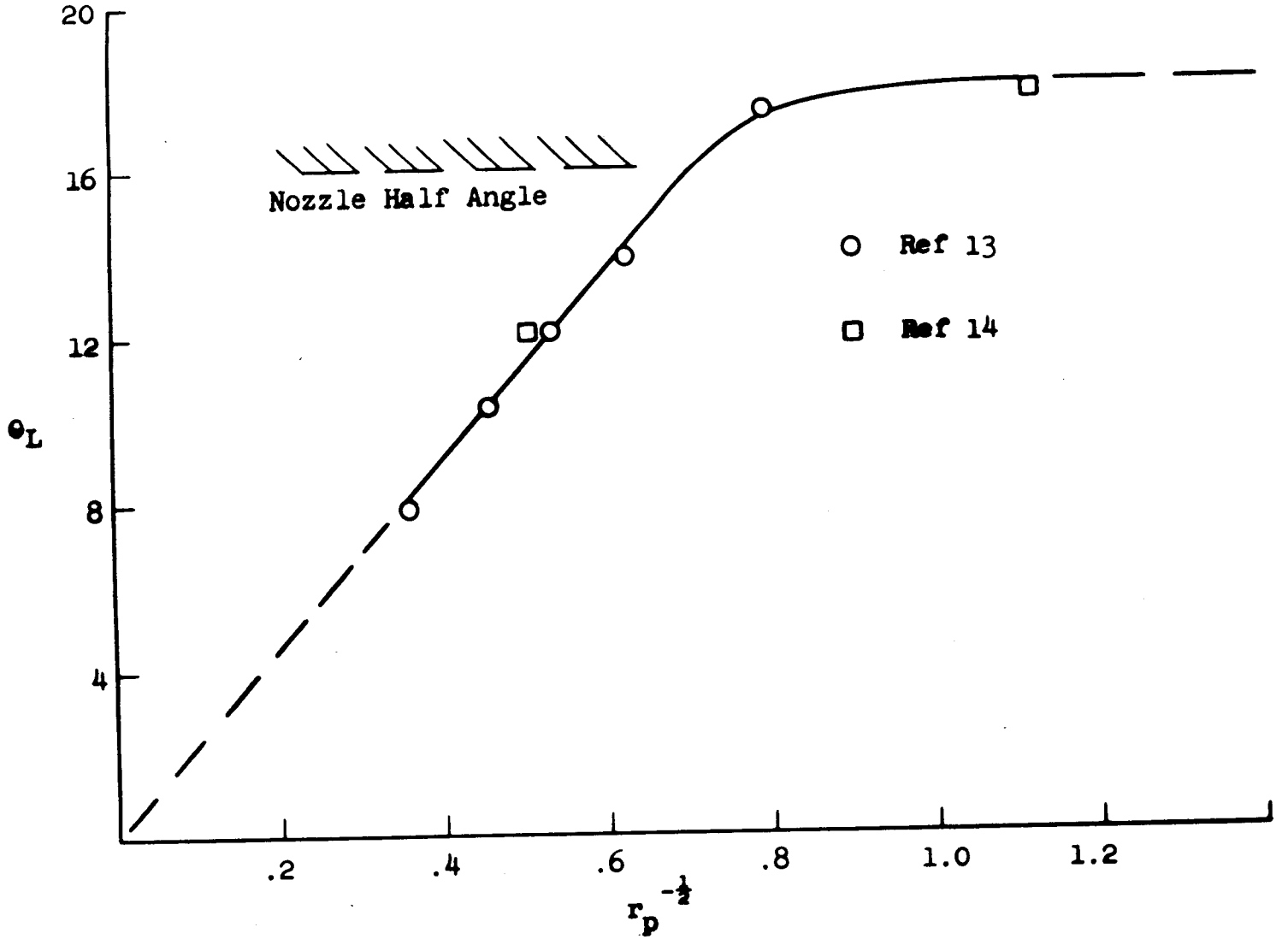

Fig 16 Limiting Particle Streamline Correlation

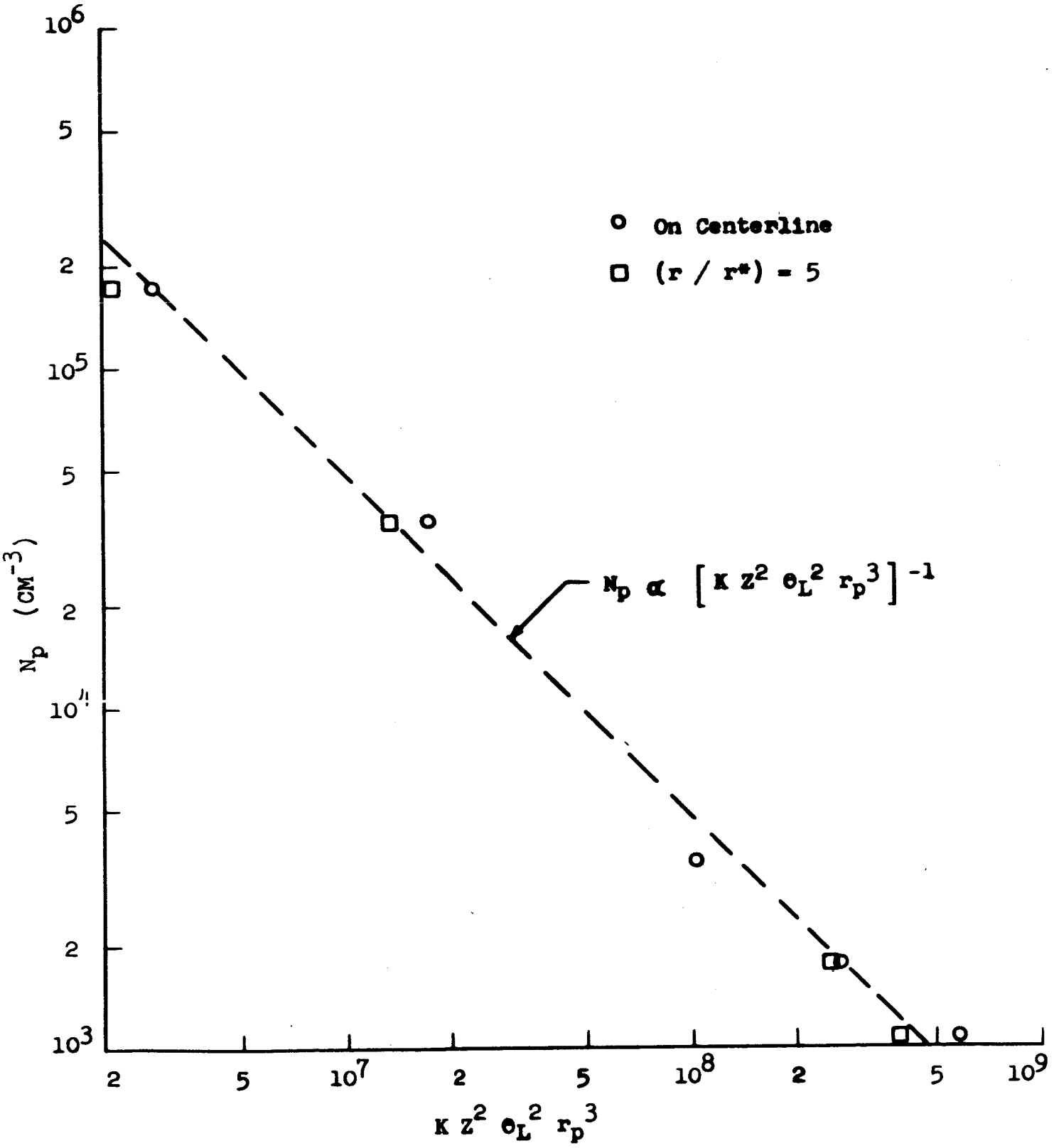

Fig 17 Particle Concentration Correlation

K. Radiative Transfer from Submicroscopic Particles (Carbon)

Because of the small size ($r_p < 1000$ Å) and high emissivity typical of carbon particles in a rocket exhaust, two important simplifications can be introduced. First, scattering of the radiation from one particle by adjacent particles can be ignored and the simple expression

$$I(\lambda) = B(\lambda,T)\left[1 - \exp(-\sigma_t N_p S)\right] \qquad (20)$$

gives the intensity received by a surface element (normal to the line of sight) from a uniform cloud of particles S units thick and having particle cross section σ_t and concentration N_p per unit volume. (See Equations 25 and 26, Reference 9). From Equation 17 and the formula for the mass of a sphere of radius r_p

$$\sigma_t N_p = \frac{6.05\times10^5}{\lambda^2}\frac{3}{4\pi\rho_p} = \frac{1.45\times10^5 W_p}{\lambda^2\rho_p} = \mu_p \qquad (21)$$

Thus the particle cloud can be considered to have an effective absorption coefficient, μ_p, which is proportional to the mass concentration of carbon W_p (in grains per cubic centimeter) and inversely proportional to the wave length(in microns). For a non-uniform cloud, the difference form of Equation 20 should be employed:

$$I_2 = B\left[1 - \exp(-\mu_p \Delta S) + I_1 \exp(-\mu_p \Delta S)\right. \qquad (22)$$

Secondly, the correlations described previously show that submicroscopic particles are, for practical purposes,in equilibrium with the gas stream and their velocity, temperature and concentration can be treated in the same manner as is done for molecular constituents.

L. Radiative Transfer from Micron-Sized Particles (Al_2O_3, MgO)

Morizumi and Carpenter (Reference 10) have carried out calculations of radiative heat transfer from Al_2O_3 particles, including the effects of scattering. They make the assumption that total cross section is a constant, $2\pi r_p^2$, thus making it possible to work with total rather than spectral intensities. They compute apparent emissivity ϵ_A for two particle geometries, an infinite slab and an infinite cylinder. Both yield the same limiting value of apparent emissivity $\epsilon_A = \epsilon_p^{\frac{1}{4}}$ when the optical thickness $\tau = N_p \sigma_t L$ is very large. L is the thickness of the slab or diameter of the cylinder. At small τ

$$\epsilon_A = 2/3\ \epsilon_p\ \tau \qquad \text{(for a cylinder)}$$

$$\epsilon_A = 2\ \epsilon_p\ \tau \qquad \text{(for a slab)}$$

At all values of τ, their results can be represented fairly accurately by the expression

$$\epsilon_A = \epsilon_p^{1/4} \left[1 - \exp\left(-C \epsilon_p^{3/4} \tau\right)\right] \qquad (23)$$

where C equals 2/3 for a cylinder and 2 for a slab. The radiant heat transfer to a surface element from a small portion of the plume is given by

$$\Delta P = \Delta F \, \epsilon_A \, \sigma \, T_p^4 \qquad (24)$$

where ΔF is the shape factor between the portion of the particle cloud in question and the element. The total radiant heat transfer is the sum of the individual contributions. No computer program has been developed at S&ID to apply Equation 24 to the geometry of an actual particle cloud of micron-sized particles. However, its use is straight forward provided the correct values of ϵ_A are available.

As an illustration of the use of Figures 14, 15, 16 and Equations 19, 23, and 24 to obtain radiant heat transfer, consider the following idealized case. The surface element in question is oriented so that its normal is perpendicular to, and passes through the plume axis. Moreover, assume that the element is located just at the edge of the plume 40 nozzle throat radii downstream of the throat. Under these circumstances the shape factor ΔF is unity and the plume properties to be used in Equation 14 are those occurring at $Z = 40r^*$.

Let the exit temperature be 1000°K, the chamber temperature be 3000°K, and the gas exit velocity (at $Z = 10r^*$) be 3×10^5 centimeters per second. Assume a nozzle throat radius of 5 centimeters and a total mass flow of 5×10^4 grams per second of which 20 percent is made up of 3 micron Al_2O_3 particles.

The velocity lag parameter at the nozzle exit is

$$r_p / \left[(r^*)^{1/2} Z^{1/4}\right] = 3.0 / \left[5^{1/2} (5 \times 10)^{1/4}\right] = 0.60$$

from which $1 - K = 0.065$ from Figure 14. (At larger values of the parameter the lower curve from Figure 14 is probably more accurate.)

The temperature lag at the exit is found to be 0.32 from Figure 15 at

$$\sqrt{r_p} = \sqrt{3} = 1.73.$$

$$T_p = t_g + (T_{go} - T_g) \times 0.32$$

$$= 1000 + (3000-1000) \times 0.32 - 1640°K$$

Since both drag and heat transfer are greatly reduced in the plume beyond the exit due to rapid gas expansion the exit values of temperature and velocity can be assumed approximately constant thereafter.

The limiting conical half-angle for the particle cloud in the plume (at $1/\overline{r_p} = 0.58$) is $\theta_L = 13.1°$ from Figure 16. Taking the particle density at the room temperature value 3.85 grams per cubic centimeter, the particle concentration can be evaluated at $Z = 40r^*$ from Equation 19.

$$N_p = \frac{0.2 \times 5 \times 10^4}{4/3\ \pi^2 \times 3.85 \times 3 \times 10^5} \frac{1}{(3 \times 10^{-4})^3 (1-0.065)(40 \times 5)^2 (\frac{13.1}{57.3})^2}$$

$$= 1.26 \times 10^4 \text{ cm}^{-3}$$

(Note that r_p must be in centimeters and θ_L in radians in Equation 19.)

The optical thickness τ is proportional to the local diameter of the conical particle cloud.

$$L = 2\ Z \tan \theta_L$$

$$= 2 \times 40 \times 5 \times .2325 = 93 \text{ cm}$$

Thus

$$\tau = N_p\ \sigma_t\ L = N_p \times 2\ \pi r_p^2\ L$$

$$= 1.26 \times 10^4 \times 2\ \pi (3 \times 10^{-4})^2 \times 93$$

$$= 0.66$$

The effective emissivity can now be calculated from Equation 23. Taking $\epsilon_p = 0.25$ and $C = 2/3$ (for a cylinder)

$$\epsilon_A = 0.25^{\frac{1}{4}} \left[1 - \exp\ (-2/3 \times .25^{3/4} \times .66)\right]$$

$$= 0.102$$

The radiant power received is then obtained from Equation .

$$\Delta P = 1.0 \times 0.102 \times 5.66 \times 10^{-12} \times (1640)^4$$

$$= 4.15 \text{ watts/cm}^2$$

M. Estimated Radiation Heating During Saturn Launch

The methods described above are being used to make representative calculations of radiant heat transfer during sea level launch of the Saturn vehicle. As described in Section V, total heat transfer measurements made on the launch structure are available which may be compared with analytical predictions of radiative and convective rates.

The instrumented locations chosen for initial radiation calculations are designated 15B1, 2 (Data Point No. 2). The procedure employed was to calculate heat transfer from the nearest engine plume only and to multiply this by a factor estimated from the additional solid angle subtended by the other plumes and the assumption that each plume is optically thick. The relevant geometrical factors for three different launch times are as follows:

time from launch (seconds)	2.0	2.8	3.8
axial location of 15B1, 2(x/R_e)	9.2	20.3	35.1
radial location of 15B1, 2(R/R_e)	(-)1.1	0.0(+)	1.6
factor (for multiplume estimate)	1.0	1.0	2.0

Calculations are being carried out using the program REDJET and the sub program REDRAD. In addition to making the geometrical correction referred to earlier, these programs were modified to accomodate the special features of a low-altitude plume.

Properties were handled in the following way. Temperature was taken constant at any axial station and assumed to vary linearly with axial station. Composition was taken to be constant within the plume and submicroscopic carbon particles were added as an additional constituent. The properties assigned at two axial stations were as follows:

Axial station (x/R_e)	0	50
Temperature (°K)	1670	1390
Pressure (atm)	1	1
Plume width (R_m/R_e)	1	1.5

Axial Station x/R_e	0	50
Gas composition (Mol fraction):		
H_2O	.38	.38
CO	.38	.38
CO_2	.12	.12
Carbon concentration (assumed weight fraction)	.01	.01

The results of the plume radiation calculations will be given in a later report.

VIII. DISCUSSION OF RESULTS AND RECOMMENDATIONS FOR FUTURE WORK

This second quarterly progress report includes a major part of the Phase II Analytical and Experimental Correlation, together with a number of the remaining topics of the Phase I Analytical Investigations. The latter include the effect of shifting specific heat ratio on free flow field jet plumes, the construction of sea level plumes and curves of properties, and radiation from solid particles.

The results of the shifting specific heat ratio study indicate that an appreciable decrease in the width of the plume boundary occurs compared with the boundary width obtained by use of an assumed constant specific heat ratio. Apparently, the principal cause of the shift in level to higher values of the specific heat ratio is the reduction in temperature as the gas expands; hence, little other difference resulted from the choice of equilibrium composition, frozen chamber composition, or a combined equilibrium frozen case where predetermined "freezing point" criteria caused the program to shift from the equilibrium to the frozen condition. Some additional study is needed to conclude that the constant nozzle exit value of specific heat ratio will provide accuracy adequate for most applications.

The equations presented in the first quarterly progress report for incorporating the Newtonian impact pressure of the freestream as an added restriction for computing the jet plume for a moving nozzle were used successfully with the Apollo AP 214 program during the past report period. The resulting compressed jet boundaries were converted to dimensionless contraction ratios in order to show trend effects for prediction purposes. Continued effort is recommended to obtain sufficient data to generalize these trends.

The empirical sea level plume decay ratios for pressure, temperature difference, and velocity were abstracted from seven experimentally-based distribution curves in the key paper on the subject by Anderson and Johns and are given in the present report in condensed tables on one sheet for ready reference while making computations. That accuracy was not lost by this practical conversion is demonstrated by the remarkably good correlation obtained between the resulting predicted impact pressures and the test data for the SA5 launch. Not such good correlation was obtained for the predicted convective heat transfer. Continued analysis is recommended to improve the correlation.

The question of the plume radiation contributing a larger portion of the total heat load measured than accounted for in the equations was investigated. The radiation from solid particles is considered, with a sample case worked out in detail to clarify the parameters involved. The

study is not yet complete; however, the level of radiation flux is expected to be far smaller than obtained by convection heat transfer. Continued investigation in this area is recommended.

In general, the present predication methods appear to give reasonably good correlation with plume impingement data obtained in high altitude test chambers, and also for the impact pressures for sea level plumes. However, because of the largely empirical nature of the methods, further study is needed and recommended to improve them, particularly in the heat transfer area for low-altitude plumes.

IX. REFERENCES

1. SID 64-1896: Engineering Method to Predict Saturn V Vehicle and Launch Complex Environments due to Rocket Jet Impingement, Quarterly Progress Report No. 1 on Contract NAS 8-11407, 15 October 1964, North American Aviation, Inc., Space and Information Systems Division.

2. NASA/MSFC letter, J. C. Cody to A. Africano, R-P&VE-PTE-64-L-99, dated 2 December 1964, and attached SA5-SA6 launch test data on impingement forces and heat loads.

3. Anderson, A. R., and F. R. Johns: Characteristics of Free Supersonic Jets Exhausting Into Quiescent Air, Jet Propulsion, Jan. 1955.

4. Love, E. S., Grigsby, C. E., Lee, L. P., and Woodling, M. J.: Experimental and Theoretical Studies of Axisymmetric Free Jets, NASA Report TR R-6, 1959.

5. Adamson, T. C. Jr., The Structure of the Rocket Exhaust Plume Without Reaction at Various Altitudes, BAMIRAC Report 4613-45-T, June 1963, University of Michigan.

6. SID 63-1520: High-Vacuum Plume Impingement Test Report, February 1964, NAA/S&ID.

7. SID 64-1563: High-Vacuum Plume Impingement Test Correlation, August 1964, NAA/S&ID, Contract NAS 9-150.

8. Kemp, H. H., and F. R. Riddell: Heat Transfer to Satellite Vehicle Reentry Vehicles Reentering the Atmosphere, Jet Propulsion, Feb. 1957.

9. Stull, R. V., and G. N. Plass: Emissivity of Dispersed Carbon Particles, Jour. Optical Society of America, v. 50 n. 2, February 1960.

10. Morizumi, S. J. and H. J. Carpenter: Thermal Radiation from the Exhaust Plume of an Aluminized Composite Propellant Rocket, Reprint No. 64-61, presented at the AIAA First Aerospace Sciences Meeting, New York, January 20-22, 1964.

11. Plass, G. N.: Mie Scattering and Absorption Cross-Sections for Aluminum Oxide and Magnesium Oxide, Applied Optics, v. 3, n. 7, July 1964.

12. Gryvnak, D. A., and D. E. Burch: Optical and Infrared Properties of Al_2O_3 at Elevated Temperatures, Philco Res. Laboratories, Report V-2623, May 1964

13. Kliegel, J. R.: Gas Particle Nozzle Flows, Ninth Symposium (International) on Combustion, Academic Press, New York, 1963.

14. Carlson, D. J., and R. F. Hoglund: Particle Drag & Heat Transfer in Rocket Nozzles, AIAA Journal v. 2, n. 11, December 1964.